^{13}C and ^{15}N Chemical Shift Tensors of Para-Substituted Benzonitriles

Maziar Sardashti and Gary E. Maciel*

Department of Chemistry, Colorado State University, Ft. Collins, Colorado 80523
(Received: December 17, 1987)

The principal elements of the ^{13}C and ^{15}N chemical shift tensors of a series of 10 para-substituted benzonitriles, enriched in ^{15}N, have been determined. For the ^{15}N case the static powder patterns and spinning sideband methods have been employed and compared. For the ^{13}C case, the two-dimensional Fourier Transform "flipper" and spinning sideband methods were employed and compared. Each method suffers from the effects of dipolar interactions with nearby nuclei, especially those that are quadrupolar. No evidence is found for compelling empirical correlations between the individual tensor elements, or such combinations of them as the asymmetry or anisotropy parameters, and traditional chemical reactivity parameters employed in linear free energy relationships. Pople's independent-electron molecular orbital perturbation theory is useful in understanding the gross relationships between chemical structure and chemical shift tensor elements and in explaining why certain tensor elements show the largest or smallest resonance-withdrawing or resonance-donating effects of substituents.

Introduction

Chemical shift values have been examined with respect to possible correlations with chemical structure and reactivity parameters for approximately 30 years.[1-10] Initially these efforts were directed toward proton chemical shifts and then the chemical shifts of ^{19}F,[5] ^{13}C,[1-4,6-10] and other nuclides, and were limited to consideration of the isotropic average, σ_i, of the chemical shift tensor. Possible correlations of σ_i values, especially in terms of substituent effects, were explored early with substituent electronegativities,[1-3] reactivity parameters,[5,10] and estimated electron densities.[3,7] This concentration of attention on σ_i resulted from the fact that until recently nearly all NMR studies by chemists were limited to liquid samples, in which Brownian motion provides isotropic averaging of the chemical shift tensor, yielding the σ_i value directly in the experimental measurement.

The successful effort in solid-state NMR during the past few years has broadened appreciation of the chemical shift to include attention on its orientation dependence, or anisotropy.[11-15] The chemical shift anisotropy (CSA) is characterized mathematically by the chemical shift tensor, σ, which can be expressed in terms of the laboratory axis system (x,y,z) by means of a 3×3 matrix:

$$\sigma = \begin{pmatrix} \sigma_{xx} & \sigma_{xy} & \sigma_{xz} \\ \sigma_{yx} & \sigma_{yy} & \sigma_{yz} \\ \sigma_{zx} & \sigma_{zy} & \sigma_{zz} \end{pmatrix} \tag{1a}$$

where the isotropic average of σ is given by

$$\sigma_{iso} = \tfrac{1}{3}(\sigma_{xx} + \sigma_{yy} + \sigma_{zz}) \tag{1b}$$

From the fundamental point of view of examining relationships between chemical structure and chemical shifts, the *principal axis system* is most convenient for representing the chemical shift tensor. In this axis system, σ takes the diagonal form:

$$\sigma = \begin{pmatrix} \sigma_{11} & 0 & 0 \\ 0 & \sigma_{22} & 0 \\ 0 & 0 & \sigma_{33} \end{pmatrix} \tag{2a}$$

where the principal tensor elements σ_{kk} are defined by the relationship

$$|\sigma_{33} - \sigma_{iso}| \geq |\sigma_{11} - \sigma_{iso}| \geq |\sigma_{22} - \sigma_{iso}| \tag{2b}$$

and where the isotropic average is now given by the equation

$$\sigma_{iso} = \tfrac{1}{3}(\sigma_{11} + \sigma_{22} + \sigma_{33}) \tag{2c}$$

In terms of these quantities the anisotropy parameter δ can be defined by

$$\delta = \sigma_{33} - \tfrac{1}{2}(\sigma_{11} + \sigma_{22}) \tag{2d}$$

and the asymmetry parameter η by

$$\eta = \frac{\sigma_{22} - \sigma_{11}}{\sigma_{33} - \sigma_{11}} \tag{2e}$$

One can see from eq 2c that knowledge of the three principal elements of the chemical shift tensor (σ_{11}, σ_{22}, σ_{33}) provides more information than just the average of these three parameters. Hence, whether one is simply trying to use the chemical shift for empirical purposes, say structure determination by empirical structure/shift relationships, or attempting to make correlations between chemical shifts and molecular or electronic structure or chemical reactivity parrameters, it would appear a priori that correlations with the individual parameters (σ_{11}, σ_{22}, σ_{33}) should be more attractive to examine.

Individual values of σ_{11}, σ_{22} and σ_{33}, as well as the orientations of their corresponding principal axes, can be obtained from experiments on the orientation dependence of the chemical shifts in single crystals.[16-18] Static powder samples provide the σ_{kk} values from the CSA "powder patterns", as indicated in Figure 1a,b, if the system is chemically simple enough so that the powder patterns of individual resonances do not overlap. For cases of relatively simple spectra that consist of well-separated, sharp lines, analysis of the spinning sideband (SSB) intensities of magic-angle spinning (MAS) experiments can yield values of σ_{11}, σ_{22}, and σ_{33} for each individual structural situation (i.e., for each σ_i value).[19-21] For more complex systems, two-dimensional FT experiments have been

* Author to whom correspondence should be addressed.

(1) Lauterbur, P. C. *J. Am. Chem. Soc.* **1961**, *83*, 1846.
(2) Savitsky, G. B.; Namikawa, K. *J. Phys. Chem.* **1964**, *68*, 1956.
(3) Spiesecke, H.; Schneider, W. G. *J. Chem. Phys.* **1961**, *35*, 772.
(4) Maciel, G. E. In *Topics in Carbon-13 NMR Spectroscopy*; Levy, G. C., Ed.; Wiley: New York, 1974; Vol. 1, p 54.
(5) Maciel, G. E.; Natterstad, J. J. *J. Chem. Phys.* **1965**, *42*, 2427.
(6) Traficante, D. D.; Maciel, G. E. *J. Phys. Chem.* **1965**, *69*, 1348.
(7) Nelson, G. L.; Levy, G. C.; Cargioli, J. D. *J. Am. Chem. Soc.* **1972**, *94*, 3088.
(8) Maciel, G. E.; Dorn, H. C. *J. Am. Chem. Soc.* **1971**, *93*, 1268.
(9) Savitsky, G. B.; Ellis, P. D.; Namikawa, K.; Maciel, G. E. *J. Chem. Phys.* **1968**, *49*, 2395.
(10) Taft, Jr., R. W.; Glick, R. E.; Lewis, I. C.; Fox, I. R.; Ehrenson, S. *J. Am. Chem. Soc.* **1963**, *85*, 709.
(11) Haeberlen, U. *High Resolution NMR in Solids. Selective Averaging*; Academic: New York, 1976.
(12) Veeman, W. S. *Prog. NMR Spectrosc.* **1984**, *16*, 193.
(13) Facelli, J. C.; Grant, D. M.; Michl, J. *Acc. Chem. Res.* **1987**, *20*, 152.
(14) Fyfe, C. A. *Solid State NMR for Chemists*; CFC Press: Guelph, Ontario, 1983.
(15) Mehring, M. *Principles of High Resolution NMR in Solids*, 2nd ed.; Springer-Verlag: Berlin-Heidelberg, 1983.
(16) Kempf, J.; Spiess, H. W.; Haeberlen, U.; Zimmermann, H. *Chem. Phys. Lett.* **1972**, *17*, 39.
(17) Pausak, S.; Tegenfeldt, J.; Waugh, J. S. *J. Chem. Phys.* **1974**, *61*, 1338.
(18) Griffin, R. G.; Pines, A.; Pausak, S.; Waugh, J. S. *J. Chem. Phys.* **1975**, *63*, 1267.
(19) Herzfeld, J.; Berger, A. *J. Chem. Phys.* **1980**, *73*, 6021.
(20) Maricq, M. M.; Waugh, J. S. *J. Chem. Phys.* **1970**, *70*, 3300.
(21) Marchetti, P. S.; Ellis, P. D.; Bryant, R. G. *J. Am. Chem. Soc.* **1985**, *107*, 8191.

0022-3654/88/2092-4620$01.50/0 © 1988 American Chemical Society

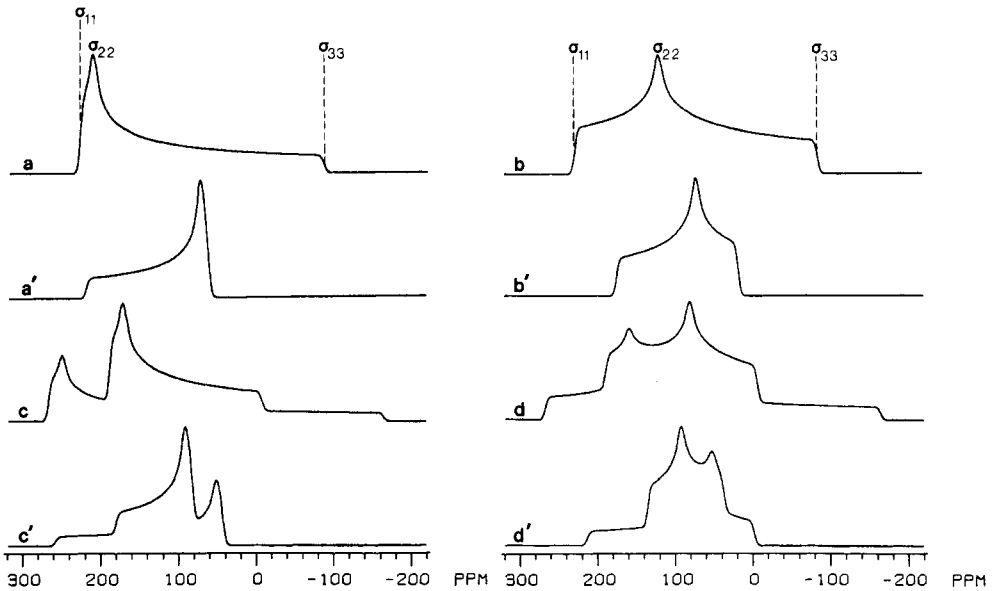

Figure 1. Representative, theoretically calculated CSA powder patterns for nearly axially symmetric case ($\eta = 0.09$) and nonaxial case ($\eta = 0.63$), showing corresponding relationship to σ_{11}, σ_{22}, and σ_{33} values. (a) Nearly axially symmetric case. (b) Asymmetric case. (a') Axially symmetric case, for spinning at 90° relative to $\mathbf{B}_0$. (b') Asymmetric case, for spinning at 90° relative to $\mathbf{B}_0$. (c) Axially symmetric case, with dipolar coupling to a spin-$^1/_2$ nucleus. (d) Asymmetric case, with dipolar coupling to a spin-$^1/_2$ nucleus. (c') Case c spinning at 90° relative to $\mathbf{B}_0$. (d') Case d with spinning at 90° relative to $\mathbf{B}_0$.

developed to provide CSA powder patterns (and, hence, σ_{11}, σ_{22}, and σ_{33} values) for all the individual σ_i values represented in the MAS spectrum.[22-24] Values of the principal chemical shift tensor elements have also been obtained from high-resolution experiments on solutes in liquid crystal solvents.[25-28]

In the work described in the present paper, σ_{11}, σ_{22}, and σ_{33} values of the ^{13}C and ^{15}N resonances in para-substituted benzonitriles (I) were determined on powdered samples. ^{15}N powder

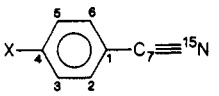

I

patterns were obtained from experiments on static samples, and ^{13}C powder patterns by means of the 2D FT "angle-flipper" technique.[23] The spinning sideband technique was also used to obtain σ_{11}, σ_{22}, and σ_{33} values.[19-21] The ranges of applicability of all these methods are compared wherever possible. The σ_{kk} values are discussed with respect to the factors that determine chemical shifts and are explored in terms of chemical structure and reactivity parameters.

Experimental Section

Materials. All para-substituted benzaldehydes and para-substituted benzoyl chlorides were obtained from Aldrich Chemical Co. and were used without further purification. Phosphorus pentoxide, hydroxylamine hydrochloride, and methyl iodide (99%) were obtained from Fisher Scientific, acetic acid (glacial) was obtained from J. T. Baker Co., durene and benzoic acid were from Eastman Kodak, and phosphoric acid (85%) was from EM Science; all were used without further purification.

^{15}N-labeled hydroxylamine hydrochloride (99% isotopic label) was obtained from both MSD and Cambridge Isotopes Laboratories. ^{15}N-labeled ammonia gas (99% isotopic label) was obtained from Cambridge Isotopes Laboratories.

TABLE I: Synthesized Para-Substituted ^{15}N-Labeled Benzonitriles

para substituent	synthetic method	mp,[30] °C found	mp,[30] °C lit.	ref	% yield
$-OCH_3$	A	58–59	57–59	29	70
$-NMe_2$	A	74–75	73–75	29	70
$-NO_2$	A	144–146	146–149	29	80
$-CN$	A	223–225	224–229	29	85
$-Cl$	A	92–94	94–96	29	70
$-Br$	A	111–112	114	29	86
$-F$	B	34–35	35–37	31	60
$-CH_3$	B	29–30	29.5	31	65
$-CMe_3$	B	5–8	*b*	31	60
$-N^+Me_3I^-$ [a]	A	157–159	160–163	32	70

[a] Prepared by methylation of Me_2N derivative with CH_3I. [b] No literature data available.

The para-substituted benzonitriles used for NMR studies, both unlabeled and the ^{15}N-labeled, were made by one of the two synthetic methods (A, B) described below. Purities of these compounds were determined by their melting points and also from ^1H NMR spectra.

Each para-substituted benzonitrile was prepared (A) from the corresponding para-substituted benzaldehyde by reaction with hydroxylamine hydrochloride under highly acidic conditions, as described previously,[29] or (B) from the corresponding para-substituted benzoyl chloride by a two-step procedure involving conversion of the benzoyl chloride to the corresponding amide by reaction with ammonia in ether and subsequent conversion of the resulting amide to the corresponding benzonitrile by P_2O_5. In a typical procedure for scheme B, a solution of 4.5 mmol of the para-substituted benzoyl chloride in 5 mL of dry ether, contained in a 25-mL three-neck flask equipped with a dry-ice condensor, was cooled in a liquid nitrogen bath and then the system was evacuated at 10^{-3} Torr. A 200-mL (9.0 mmol) portion of NH_3 gas was transferred via vacuum line into the reaction mixture, which was then allowed to warm to room temperature under reflux conditions, using a dry-ice condenser. The resulting white precipitate (NH_4Cl, plus the amide) was first washed with 20 mL of ether to remove the original acyl chloride and then filtered. To the residue was added 50 mL of acetone, and the mixture was stirred at room temperature for 15 min before a final filtration to remove NH_4Cl. The solvent was removed from the filtrate on

(22) Bax, A.; Szeverenyi, N. M.; Maciel, G. E. *J. Magn. Reson.* **1983**, *51*, 400.
(23) Bax, A.; Szeverenyi, N. M.; Maciel, G. E. *J. Magn. Reson.* **1983**, *55*, 494.
(24) Maciel, G. E.; Szeverenyi, N. M.; Sardashti, M. *J. Magn. Reson.* **1985**, *64*, 365.
(25) Fung, B. M. *J. Am. Chem. Soc.* **1983**, *105*, 5713.
(26) Fung, B. M.; Kong, C. F. *J. Am. Chem. Soc.* **1984**, *106*, 6193.
(27) Parhami, P.; Fung, B. M. *J. Am. Chem. Soc.* **1985**, *107*, 7304.
(28) Fung, B. M.; Parhami, P. *J. Magn. Reson.* **1985**, *63*, 168.
(29) Ganoba, I.; Pamolo, C. *Synth. Commun.* **1983**, *13*, 999.

TABLE II: ^{15}N Chemical Shift Tensor Elements of Para-Substituted Benzonitriles[a]

X	σ_{aa}		σ_{bb}		σ_{cc}				δ^f		η^g	
	static[b]	SSB[c]	static	SSB	static	SSB	σ_{iso}[d]	σ_i[e]	static	SSB	static	SSB
$-NMe_2$	396.6 ± 0.0	404.9 ± 8.9	355.7 ± 0.7	347.8 ± 8.0	5.3 ± 3.1	7.2 ± 1.5	252.5 ± 1.2	253.2	−371	−369	0.17	0.23
$-OCH_3$	393.0 ± 1.1	390.7 ± 3.6	359.1 ± 0.8	359.1 ± 0.8	7.0 ± 1.9	2.6 ± 3.7	253.0 ± 0.0	253.4	−369	−376	0.14	0.10
$-CH_3$	396.1 ± 0.1	385.3 ± 5.0	367.3 ± 0.2	370.7 ± 3.1	0.8 ± 0.9	9.1 ± 2.0	254.7 ± 0.3	254.4	−381	−369	0.11	0.059
−F	393.9 ± 0.4	385.2 ± 2.0	370.5 ± 0.7	377.2 ± 3.0	2.1 ± 1.4	5.6 ± 1.6	255.5 ± 0.6	257.4	−380	−376	0.092	0.032
−Cl	395.5 ± 0.1	387.6 ± 3.9	371.4 ± 1.4	381.9 ± 2.0	5.4 ± 0.1	1.6 ± 5.5	257.4 ± 0.6	258.1	−378	−383	0.097	0.022
−Br	398.2 ± 0.6	390.9 ± 3.9	374.2 ± 0.9	377.6 ± 9.4	4.5 ± 1.3	3.5 ± 6.5	258.2 ± 0.6	258.6	−382	−383	0.095	0.038
$-CMe_3$	398.3 ± 0.3	393.0 ± 9.1	374.7 ± 0.4	382.1 ± 5.1	2.3 ± 1.0	−0.6 ± 10.7	258.4 ± 0.3	258.1	−384	−388	0.092	0.042
−CN	393.6 ± 3.0	392.5 ± 4.4	380.2 ± 0.2	384.1 ± 7.8	5.7 ± 2.6	8.9 ± 6.5	259.8 ± 2.0	261.9	−381	−380	0.053	0.034
$-N^+Me_3I^-$	403.4 ± 0.4	402.4 ± 6.5	382.7 ± 1.1	386.3 ± 5.5	12.1 ± 1.3	9.2 ± 6.9	266.0 ± 0.0	264.8	−381	−385	0.082	0.061
$-NO_2$	397.9 ± 1.1	390.2 + 4.5	386.8 ± 0.4	388.1 ± 4.6	4.3 ± 1.1	10.7 ± 9.0	263.0 ± 0.1	262.8	−379	−378	0.043	0.009

[a] Values in ppm relative to the chemical shift of $NH_3(l)$ at 0 ppm, with standard deviations (based on duplicate or triplicate runs) indicated. Algebraically larger numbers correspond to lower shieldings. For these data $\sigma_{aa} = \sigma_{11}$, $\sigma_{bb} = \sigma_{22}$, and $\sigma_{cc} = \sigma_{33}$. [b] Values obtained from static powder pattern. [c] Values obtained from analysis of spinning sideband (SSB) intensities in the magic-angle spinning spectra. [d] $\sigma_{iso} = {}^1/_3(\sigma_{11} + \sigma_{22} + \sigma_{33})$ from the static powder pattern. [e] σ_i obtained from magic-angle spinning spectra. [f] Defined by eq 2d. [g] Defined by eq 2e.

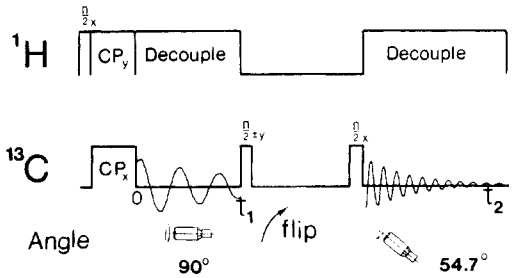

Figure 2. Timing sequence for 2D FT angle-flipping experiment.

a roto-vap, and the amide was dried at 10^{-3} Torr and 40 °C. In the conversion of the amide into a nitrile, 4.0 mmol of the dry amide was mixed with 0.75 g of P_2O_5 in a 10-mL round-bottom flask attached to a small short-path distillation apparatus. The mixture was first heated under dry N_2 (1 atm) at 120 °C for 30 min and then brought to 190 °C and distilled at 10^{-4} Torr. The collected para-substituted benzonitrile was used without further purification. Table I summarizes the yields and melting points of the ^{15}N-labeled products prepared via methods A and B.

p-Cyanophenyltrimethylammonium iodide was prepared from the corresponding *p*-(dimethylamino)benzonitrile by the reaction of 0.30 g of the former with 2.0 mL of CH_3I in 3 mL of ether and 0.05 mL of methanol at 40 °C under reflux for 14 days. The resulting precipitate, p-$(CH_3)_3N^+$–$C_6H_4CNI^-$, was washed several times with ether, providing a conversion yield of 70%, mp 157–159 °C (lit. 160–163 °C).[32]

NMR Experiments. All ^{15}N NMR spectra were obtained under cross-polarization conditions at 20.3 MHz on a lab-modified Nicolet NT-200 spectrometer, employing a Chemagnetics CP/MAS probe. The ^{13}C CP/MAS spectra used for the spinning sideband determination of σ_{11}, σ_{22}, and σ_{33} were obtained either at 50.3 MHz on the same instrument or at 90.5 MHz on a lab-modified Nicolet NT-360 spectrometer employing a "home-built" probe with a "Windmill" spinner.[33]

The ^{13}C angle-flipper experiments, employing the previously reported timing sequence shown in Figure 2,[23] were carried out at 25.3 MHz on a "home-built" 2.3-T spectrometer with a wide-bore Nalorac magnet, a Nicolet 1180 computer, a Nicolet 293B pulse programmer, and a MAS probe employing a spinner of the Chemagnetics triplet air-bearing/turbine design. The $90°_{\pm y}$ and $90°_{x}$ ^{13}C pulses shown in Figure 2 are for the purpose of "storing" ^{13}C magnetization that emerges from the evolution period (t_1) along the static magnetic field, $\mathbf{B}_0$, during the 0.25–0.35-s period during which the sample spinner axis is flipped from 90° to 54.7° (relative to $\mathbf{B}_0$) by the computer-controlled stepper motor that is mounted at the top of the probe and connected to the stator of the spinner system by means of gears and a plastic chain. The samples were spun at about 2.1–2.5 kHz. The t_1 period was incremented typically in 64 steps of 83 μs, giving a spectral width of 6 kHz and a resolution of 24 Hz in the F_1 dimension of the 2D Fourier transformed spectrum. The ^{13}C transmitter frequency was set at the high-shielding side of the ^{13}C spectrum in each case.

The chemical shift convention used in the scales shown with the ^{15}N and ^{13}C NMR spectra presented in this article is what is often referred to as the δ "scale", in which algebraically smaller (more negative) numbers represent higher shielding. The same convention is used for the chemical shift tensor elements presented in Tables II and III. For these tables and eq 1 and 2, the symbol σ is used synonymously with chemical shift, although σ is often employed in the literature to represent "shielding", with a sign convention opposite to what is employed here for σ. The symbol δ is reserved in this paper for the anisotropy, as defined in eq 2d.

Results and Discussion

^{15}N Chemical Shift Patterns. ^{15}N CSA powder patterns were obtained on the 10 ^{15}N-enriched para-substituted benzonitriles represented in Table I. The spectra are shown in Figure 3. One sees that the CSA patterns, except for that of the *p*-bromobenzonitrile, resemble those expected for a chemical shift tensor that is axially symmetric, or nearly so. Thus, as seen from Figure 1a, one can expect to extract values of σ_{11}, σ_{22}, and σ_{33} directly from the inflection points and maximum of each CSA pattern. The powder pattern that is closest to axial symmetry ($\eta = 0$) appears to be that of *p*-nitrobenzonitrile (Figure 3I), while the one with the largest apparent deviation from axial symmetry ($\eta = 0.2$) is the *p*-dimethylamino case (Figure 3A).

The ^{15}N powder pattern for *p*-bromobenzonitrile (Figure 3F) appears anomalous. The stark deviation of the line shape in this powder pattern from that of a simple CSA pattern (Figure 1a or 1b) could a priori be due to one or both of the following two possible effects: (a) an orientation dependence of pertinent cross-polarization relaxation times (i.e., T_{HN}), which could leave "holes" in segments of the powder pattern that correspond to unfavorable orientations of the pertinent internuclear ^1H–^{15}N vectors, as has been observed in the ^{13}C CP spectra of analogous systems; and (b) effects of the dipolar interactions between ^{15}N and either ^{79}Br ($I = {}^3/_2$; 50.5% natural abundance) or ^{81}Br ($I = {}^3/_2$; 49.5% natural abundance). Explanation (a) can be ruled out on the basis of variable contact-time experiments. ^{15}N "powder patterns" obtained with cross-polarization contact times ranging from 0.1 to 20 ms (spectra not shown here) all display essentially the same shape.

From single-crystal X-ray diffraction studies one knows that *p*-bromobenzonitrile molecules in the crystal line up with a head-to-tail arrangement in which the intermolecular N···Br internuclear distance is 3.27 Å.[34] Then, as the magnetogyric ratios

(30) *CRC Handbook of Chemistry and Physics*, 60th ed.; CRC Press: Boca Raton, FL, 1980.
(31) References in March, J. *Advanced Organic Chemistry*; 2nd ed.; McGraw-Hill: New York, 1977.
(32) Weley, G. R.; Miller, S. I. *J. Org. Chem.* **1972**, *37*, 767.
(33) Wind, R. A.; Anthonio, F. E.; Duijvestijn, M. J.; Smidt, J.; Trommel, J.; DeVette, G. M. C. *J. Magn. Reson.* **1983**, *52*, 424.
(34) Britton, D.; Konnert, J.; Lam, S. *Cryst. Struct. Commun.* **1977**, *6*, 45.

TABLE III: ^{13}C Chemical Shift Tensor Elements of Para-Substituted Benzonitriles[a]

substituent/ carbon	σ_{aa} flipper[b]	σ_{aa} SSB[c]	σ_{bb} flipper	σ_{bb} SSB	σ_{cc} flipper	σ_{cc} SSB	σ_{iso}[d]	σ_i[e]	σ[g] flipper	σ[g] SSB	η[h] flipper	η[h] SSB
$-NMe_2$												
C7	231.4	(237.1 ± 5.5)[f]	216.6	(191.9 ± 8.3)	−91.0	(−63.9 ± 2.8)	119.0	121.7	−315	(−278)	0.07	(0.24)
C4	(235.6)	(234.5 ± 0.60)	(180.4)	(183.0 ± 4.6)	(51.6)	(42.4 ± 4.1)	(155.8)	(153.3)	(−156)	(−166)	(0.53)	(0.46)
C1	187.1	184.2 ± 1.3	91.5	96.5 ± 0.0	10.3	8.9 ± 1.3	96.3	96.5	−129[k]	−132	1.11[k]	1.00
C2,6	231.9	232.9 ± 1.7	150.9	149.5 ± 1.3	14.7	21.2 ± 0.4	132.5	134.5	−177	−170	0.68	0.74
C3,5	187.6	189.6 ± 1.9	132.4	131.6 ± 4.0	11.0	13.6 ± 2.1	110.4	111.6	−149	−147	0.56	0.59
$-OCH_3$												
C7	228.4	(248.4 ± 4.0)	215.6	(180.1 ± 5.1)	−86.6	(−65.1 ± 1.1)	119.2	121.1	−309	(−279)	0.06	(0.25)
C4	242.8	246.7 ± 1.1	172.8	171.2 ± 1.3	68.0	67.5 ± 0.1	161.2	161.8	−140	−142	0.75	0.80
C1	195.4	195.8 ± 1.1	99.6	101.5 ± 0.0	7.4	7.2 ± 1.2	100.8	101.5	−140[k]	−142	1.03[k]	1.00
C2,6	230.7	232.0 ± 2.7	155.3	152.6 ± 0.8	15.5	16.3 ± 1.9	133.9	133.6	−178	−176	0.64	0.68
C3,5	189.3	190.7 ± 0.9	135.9	131.2 ± 1.4	10.7	8.5 ± 0.2	112.7	110.1	−152	−152	0.52	0.59
	196.0	213.2 ± 2.1	131.6	130.9 ± 0.6	19.4	10.7 ± 2.8	115.6	118.2	−144	−161	0.67	0.77
$-CH_3$												
C7	230.2	(233.6 ± 9.6)	215.4	(190.8 ± 10.7)	−92.2	(−65.8 ± 1.0)	117.8	119.5	−315	(−278)	0.071	(0.23)
C4	240.0	245.6 ± 4.3	191.0	172.1 ± 0.1	11.8	17.3 ± 4.2	144.2	145.0	−204	−192	0.37	0.58
C1	211.6	205.6 ± 2.3	112.2	110.1 ± 0.1	5.4	14.4 ± 2.3	107.8	110.0	−157	−144	0.97	1.00
C2,6,3,5[i]	228.7	218.6 ± 3.1	155.1	149.4 ± 5.8	11.7	31.0 ± 2.7	131.9	133.0	−180	−153	0.61	0.68
	227.1	218.6 ± 3.1	146.1	149.4 ± 5.8	17.3	31.0 ± 2.7	130.1	133.0	−169	−153	0.72	0.68
$-F$[j]												
C7		(248.0 ± 1.4)		(202.1 ± 0.1)		(−87.4 ± 1.3)		120.9		(312)		(0.23)
C4		238.4 ± 9.3		164.2 ± 0.1		89.7 ± 9.2		164.1		(−112)		(1.00)
C1		201.2 ± 3.6		111.5 ± 0.8		17.7 ± 4.4		110.1		−139		0.97
C2,6		206.4 ± 6.7		156.7 ± 2.1		44.2 ± 8.6		135.8		−137		0.54
C3,5		174.3 ± 5.7		131.3 ± 10.3		46.1 ± 4.6		117.2		−107		0.61
$-Cl$[j]												
C7		(232.1 ± 9.6)		(208.1 ± 21.4)		(−81.0 ± 11.9)		119.7		(−301)		(0.12)
C4		242.8 ± 3.7		142.3 ± 0.4		41.4 ± 4.0		142.2		−151		1.00
C1		213.3 ± 1.3		110.4 ± 0.3		7.2 ± 1.5		110.3		−155		1.00
C2,6		228.4 ± 1.3		146.9 ± 0.2		28.9 ± 1.6		134.7		−159		0.77
C3,5		215.5 ± 6.2		148.6 ± 2.6		27.5 ± 3.6		130.5		−155		0.66
$-Br$[j]												
C7		(227.0 ± 1.4)		(225.0 ± 1.3)		(−92.9 ± 2.8)		119.7		(−319)		(0.01)
C4,2,6,3,5[i]		220.9 ± 5.2		160.9 ± 0.5		21.8 ± 4.7		134.5		−169		0.53
C1		214.2 ± 0.5		111.9 ± 2.8		3.9 ± 3.3		110.0		−159		0.96
$-CMe_3$[j]												
C7		(238.3 ± 4.2)		(182.0 ± 4.6)		(−60.5 ± 0.4)		119.9		(−270)		(0.31)
C4		244.0 ± 0.9		213.7 ± 2.3		19.6 ± 1.5		159.1		−209		0.22
C1		203.6 ± 1.4		109.1 ± 0.0		14.5 ± 1.4		109.1		−142		1.00
C2,6		224.4 ± 1.4		155.8 ± 0.5		19.4 ± 0.9		133.2		−171		0.60
C3,5		217.2 ± 0.9		155.0 ± 0.2		11.5 ± 1.1		127.9		−175		0.53
$-CN$												
C7	227.8	(231.6 ± 17.8)	209.4	(198.4 ± 21.2)	−87.2	(−73.0 ± 3.3)	116.6	119.0	−306	(−288)	0.09	(0.17)
C4,1[i]	220.1	220.2 ± 1.8	120.9	117.1 ± 0.2	6.9	12.3 ± 1.1	115.9	116.5	−164	−156	0.91	0.99
C2,6,3,5[i]	226.3	231.6 ± 2.2	160.1	157.7 ± 2.5	9.3	9.9 ± 0.3	131.9	133.0	−184	−185	0.58	0.60
$-N^+Me_3I^-$												
C7	237.7	205.4 ± 0.6	215.5	200.7 ± 0.9	−92.1	−46.1 ± 1.1	120.3	120.0	−319	249.2	0.11	0.028
C4	231.0	235.3 ± 0.7	173.0	154.4 ± 1.9	46.0	63.9 ± 2.7	150.0	151.2	(−156)	(−131)	(0.56)	(0.93)
C1	217.7	216.3 ± 4.6	112.5	112.7 ± 0.0	6.5	9.2 ± 4.6	112.3	112.7	−159[k]	−155	0.99[k]	1.00
C2,6	204.7	191.9 ± 1.0	182.5	190.8 ± 1.0	17.1	26.8 ± 2.1	134.9	136.5	−176	−191	0.19	0.010
C3,5	190.5	187.5 ± 15.1	168.7	163.7 ± 17.0	5.9	19.4 ± 2.0	121.7	123.5	−174	−156	0.19	0.23
$-NO_2$												
C7[i]	232.7		215.9		−93.9		118.3	118.9	−318		0.079	
C4	209.9	225.9 ± 2.0	197.1	150.0 ± 0.0	72.7	74.1 ± 2.0	159.9	150.0	(−131)	(−114)	(0.15)	(1.00)
Cl[i]	215.6		133.6		20.0		123.0	118.9	−155		0.80	
C2,6	230.1	224.0 ± 8.7	162.1	160.8 ± 13.5	8.3	22.7 ± 4.8	132.7	135.8	−188	−170	0.55	0.56
	231.6	220.8 ± 1.3	160.6	157.2 ± 7.3	4.6	23.0 ± 6.0	132.2	133.6	−192	−166	0.56	0.58
C3,5	207.5	203.0 ± 1.6	164.9	161.2 ± 3.0	−0.7	9.6 ± 4.5	123.9	124.6	−187	−172	0.34	0.36

[a] Values in ppm relative to the chemical shift of TMS at 0 ppm, with standard deviations (based on duplicate or triplicate runs) indicated. Algebraically larger values correspond to lower shieldings. [b] Value obtained from angle-flipping experiments, estimated error ±3 ppm. [c] Values obtained from analysis of spinning sideband (SSB) intensities in magic-angle spinning spectra. [d] $\sigma_{iso} = {}^1/_3(\sigma_{11} + \sigma_{22} + \sigma_{33})$ from the flipper experiments. [e] σ_i obtained from magic-angle spinning spctra. [f] Values in parentheses are of questionable value, because of undetermined contributions from dipolar interactions. [g] Defined by eq 2d. [h] Defined by eq 2e. [i] Overlapped in MAS spectra. [j] No flipper data available. [k] Values obtained with the convention $\sigma_{aa} = \sigma_{11}$, $\sigma_{cc} = \sigma_{33}$, instead of that of eq 2b.

of ^{79}Br and ^{81}Br are within about 8% of each other, we can estimate the ^{15}N–Br magnetic dipolar interaction to be about 90 Hz, or about 4.5 ppm for ^{15}N, in this system, an effect that should be noticeable but not dominant in the observed ^{15}N powder pattern. It should also be noted that the quantization axis of the ^{79}Br and ^{81}Br nuclear electric quadrupole effect need not be colinear with $\mathbf{B}_0$, complicating predictions of the dipolar effects of the bromine nuclei on the ^{15}N powder pattern. If the ^{79}Br and ^{81}Br relaxation times are much shorter than about 10 ms, then the small dipolar effects of these nuclei on the ^{15}N resonance should be "self-decoupled". In any case, the origin of the unusual line shape seen in Figure 3F remains at this point unexplained. Nevertheless, values of σ_{11}, σ_{22}, and σ_{33} have been estimated from the most prominent features of the pattern.

The ^{15}N σ_{11}, σ_{22}, and σ_{33} values obtained from the static powder spectra shown in Figure 3 are summarized in Table II. One sees

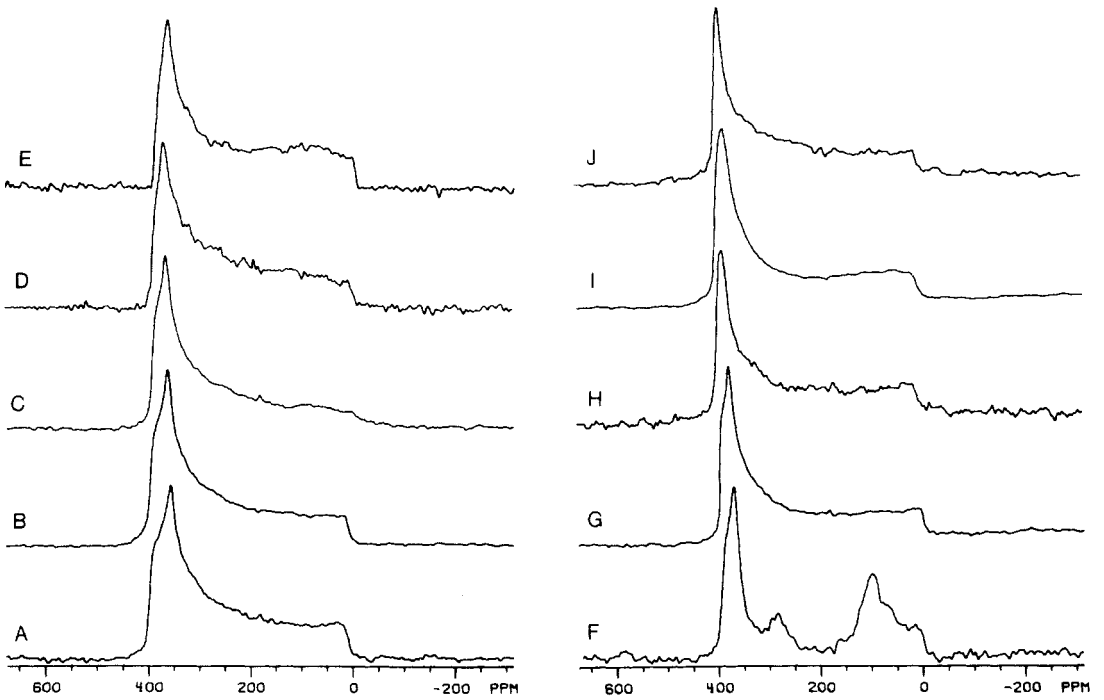

Figure 3. ^{15}N static powder spectra of para-substituted benzonitriles: (A) $-NMe_2$, (B) $-OCH_3$, (C) $-CH_3$, (D) $-F$, (E) $-Cl$, (F) $-Br$, (G) $-CMe_3$, (H) $-CN$, (I) $-N^+Me_3I^-$, (J) $-NO_2$.

that the σ_{11} values vary from compound to compound by about 10 ppm, the σ_{22} values by about 31 ppm, and the σ_{33} values by about 11 ppm. One might expect that the task of assigning the position of the maximum (corresponding to σ_{22}) in the powder pattern would be more straightforward than assigning positions to the inflection points (σ_{11} and σ_{33}) at the extremes of the powder pattern. Hence, with a greater range and anticipated greater accuracy, σ_{22} would seem to merit the most serious consideration in the discussion below. It is noteworthy that values of $\sigma_{iso} = {}^1/_3(\sigma_{11} + \sigma_{22} + \sigma_{33})$ calculated from the static powder data agree for all samples within 2.1 ppm with the σ_i values obtained from MAS experiments; in most cases the σ_{iso}-vs-σ_i agreement is within 1.0 ppm. This level of agreement provides at least a qualitative calibration on one's ability to extract σ_{kk} values from powder patterns.

CP/MAS ^{15}N spectra were obtained on the ^{15}N-labeled para-substituted benzonitriles under conditions in which the MAS speeds employed were small enough (1.0–2.5 kHz) to provide extensive spinning sidebands (SSB). Sample spectra are given in Figure 4. From the intensities in these SSB patterns, values of σ_{11}, σ_{22}, and σ_{33} were extracted, by using a computer program kindly provided by Prof. P. D. Ellis.[21] In this method the SSB pattern is obtained by Fourier transformation of the free induction decay computed as the rotational echo decay determined by a specific choice of values for δ and η, which are then varied iteratively in a SIMPLEX optimization scheme. Values of σ_{11}, σ_{22}, and σ_{33} obtained by the SSB method are also listed in Table II. Although the agreement between σ_{kk} values obtained by the SSB and static powder approaches is only qualitative, the same general pattern of results is obtained, in the following senses: (1) the range of σ_{22} values with substituent variation is much larger than the ranges computed for σ_{11} and σ_{33}; (2) while the anisotropy parameter is relatively insensitive to substituent variation, with only about a 4–5% variation with substituent changes, the asymmetry parameter ranges from about 0.2 for the case of a $-NMe_2$ substituent down to about 0.01 for the $-NO_2$ case. Both methods yield the result that, for most of these para-substituted benzonitriles, the ^{15}N chemical shift tensor is nearly axially symmetric.

The rather large values of standard deviations for the σ_{kk} values obtained by the SSB method and the poor level of agreement between corresponding σ_{kk} values obtained from the static powder pattern and SSB results summarized in Table II inspire caution in the use of the SSB technique to monitor small variations in chemical shift tensor elements, e.g., substituent effects. This statement is especially relevant for the element σ_{22}, for which the nature of a static powder pattern should render the extraction of a reliable value straightforward and precise. For these reasons, the discussion below accords less weight to the σ_{kk} values obtained by the SSB approach than to values obtained by the other methods employed in this study.

^{13}C Chemical Shift Patterns. The 2D FT "flipper" technique[23] was used to obtain ^{13}C CSA patterns on 6 of the 10 para-substituted benzonitriles listed in Table I. The assignments of σ_i values in the F_2 domain to specific structural positions in the para-substituted benzonitriles were made on the basis of comparisons to well-established liquid-sample ^{13}C chemical shift assignments, employing additivity rules.[35,36] It is interesting that deviations from additivity in the σ_i values[37] are typically less than 3 ppm in the results reported here.

In order to have a "calibration" on the reliability of results obtained by this technique, we obtained 2D FT flipper results for compounds that had been studied elsewhere by the single-crystal method or isotopic labeling. For this purpose benzoic acid and durene (1,2,4,5-tetramethylbenzene) were used.

Figures 5 and 6 display the 2D FT flipper results for benzoic acid and durene, respectively. "Slices" into the F_1 domain at specific values of F_2 yield the CSA powder patterns of interest in each of these 2D FT spectra. One should note that each of the F_1-domain CSA patterns displayed in these, and later, figures have been scaled down in size by a factor of 2 and reflected through the corresponding σ_i value. This results from the effect of spinning the sample at an angle, $\beta = 90°$, relative to $\mathbf{B}_0$ during the evolution period (t_1) of the sequence shown in Figure 2, as described by the following equation for the time-averaged observed chemical shift, $\bar{\sigma}_{zz}$, for a given crystallite in a powder (where $\sigma_{z'z'}$ reflects the chemical shift projection along the spinning axis):

$$\bar{\sigma}_{zz} - \sigma_i = {}^1/_2(3\cos^2\beta - 1)(\sigma_{z'z'} - \sigma_i) \qquad (3)$$

The benzoic acid results given in Figure 5 show four distinct "isotropic" peaks in the F_2 domain. The intense peak at 130 ppm

(35) Wehrli, F. W.; Wirthlin, T. *Interpretation of Carbon-13 NMR Spectra*; Heyden: London, 1976.
(36) Ewing, D. F. *Org. Magn. Reson.* **1979**, *12*, 499.
(37) Nagaoka, S.; Terao, T.; Imashiro, F.; Saika, A.; Hirota, N. *Chem. Phys. Lett.* **1981**, *80*, 580.

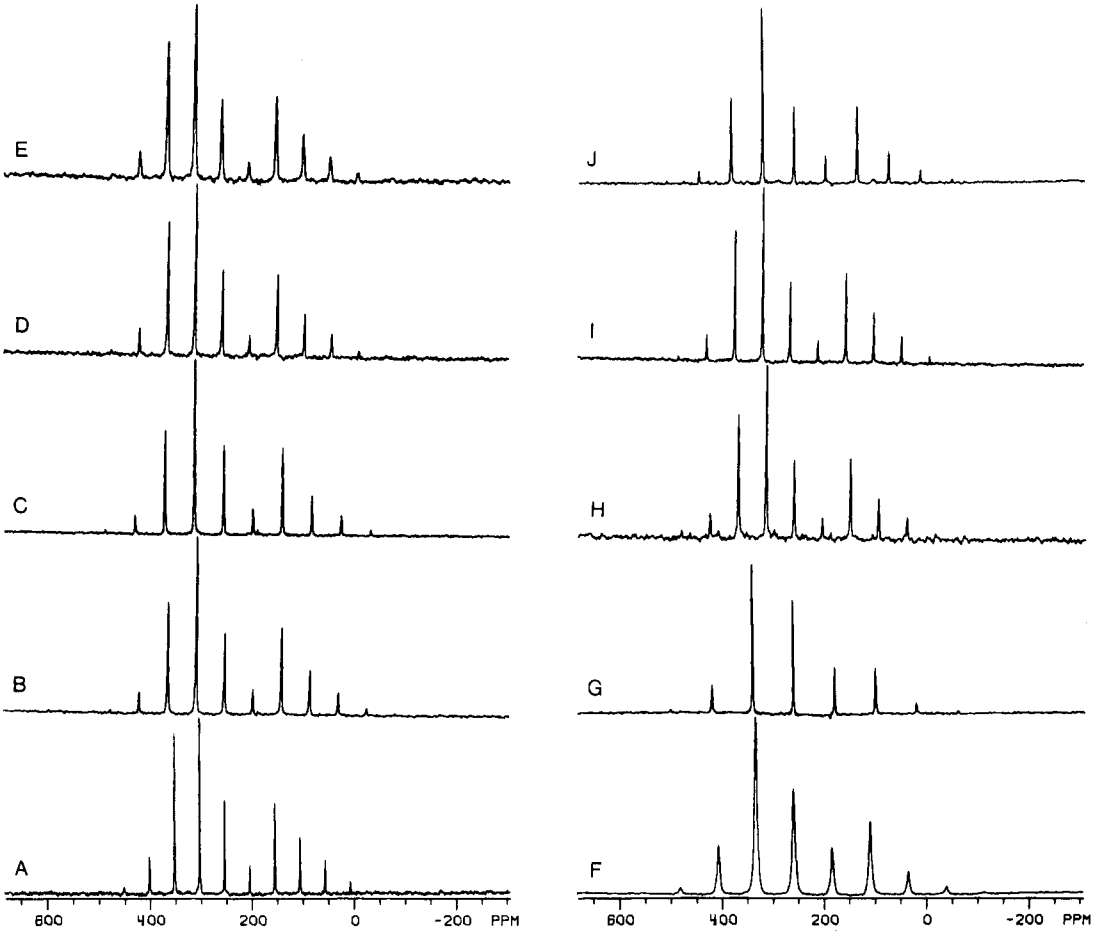

Figure 4. ^{15}N spinning sideband (SSB) spectra of para-substituted benzonitriles: (A) $-NMe_2$, (B) $-OCH_3$, (C) $-CH_3$, (D) -F, (E) -Cl, (F) -Br, (G) CMe_3, (H) -CN, (I) $-N^+Me_3I^-$, (J) $-NO_2$.

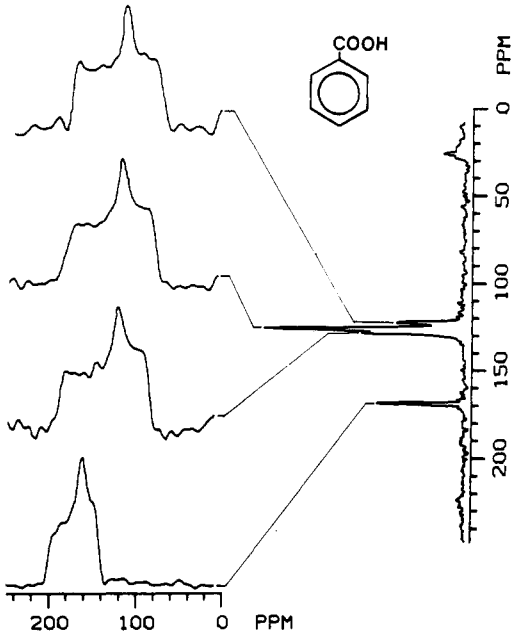

Figure 5. 2D FT ^{13}C flipper results obtained for benzoic acid.

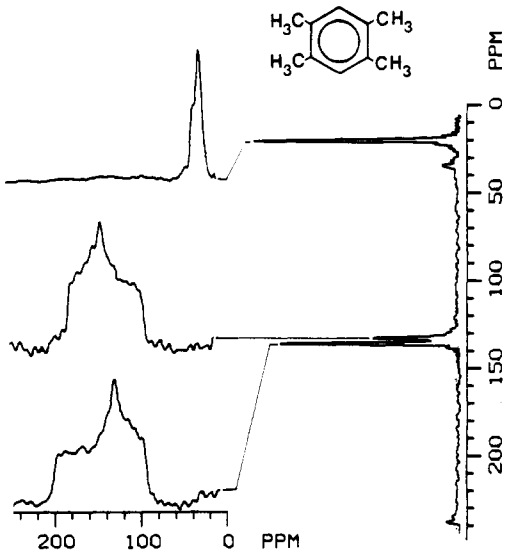

Figure 6. 2D FT ^{13}C flipper results obtained for durene.

results from the overlap of the C2, C3, C5, and C6 resonances. The C1 and C4 resonances are resolved at 127 ppm and 132 ppm, respectively, as is the C7 (carboxyl) resonance at 173 ppm. The CSA patterns in the F_1 domain display well-defined features for determining σ_{11}, σ_{22}, and σ_{33}, as well as some additional, unanticipated "minor" features. These additional maxima and minima can be due to (1) differences in cross-polarization efficiencies for specific crystallite orientations, (2) the difficulty of maintaining a truly random orientation of crystallites in a MAS experiment on a powder,[24] and (3) signal-to-noise problems associated with large ^1H T_1 values (>30 s in the benzoic acid case) that constrain the number of repetitions one can carry out in a cross-polarization experiment of specified overall duration.

Values of the principal shielding tensor elements obtained from the benzoic acid data are, listed in order of increasing shielding, C1, 223.2, 142.2, 13.6 ppm; C2, C3, C5, C6, 227.7, 147.7, 11.7; C4, 227.7, 151.4, 8.2; C7, 223.2, 187.8, 105.8, with $\sigma_{iso} = {}^1/_3(\sigma_{11} + \sigma_{22} + \sigma_{33}) = 172.2$. Results reported from experiments on a sample with ^{13}C enrichment of the carboxyl carbon (C7) are 227, 186, 107, and 173 ppm, respectively.[37] This constitutes excellent agreement between the two methods.

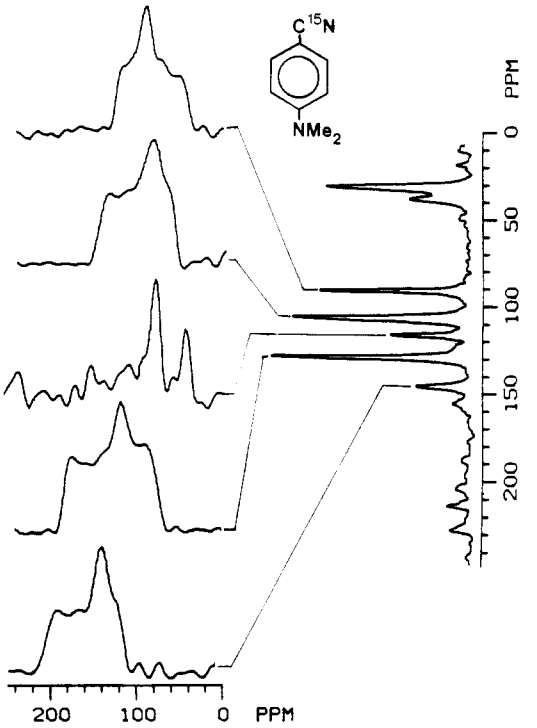

Figure 7. 2D FT ^{13}C flipper results obtained for p-Me_2N–benzonitrile.

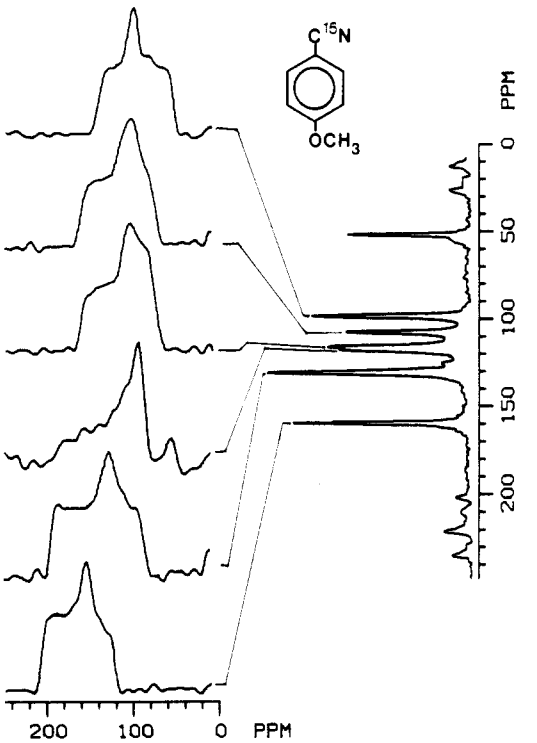

Figure 8. 2D FT ^{13}C flipper results obtained for p-CH_3O–benzonitrile.

Figure 6 shows the corresponding results for durene, 1,2,4,5-tetramethylbenzene. The CSA pattern for the methyl carbons at 19 ppm in the F_2 domain is much narrower (with principal chemical shift tensor elements 30, 23, and 3 ppm) than those observed for the aromatic carbons. For the methyl-substituted aromatic carbons (C1, C2, C4, C5) the following results were obtained for the principal chemical shift elements: 231, 157, and 15 (σ_{iso} = 134). For C3 and C6 the values are 223, 125, and 47 (σ_{iso} = 132). These results compare very favorably with those reported from single-crystal measurements:[38] CH_3, 31, 23, 3 (19); C1, C2, C4, C5, 231, 156, 16 (134); C3, C6, 223, 122, 46 (130). These patterns of agreement support the assumption that the 2D FT flipper technique yields chemical shift tensor elements that are reliable to about ±3 ppm.

(38) Pausak, S.; Pines, A.; Waugh, J. S. *J. Chem. Phys.* **1973**, *59*, 591.

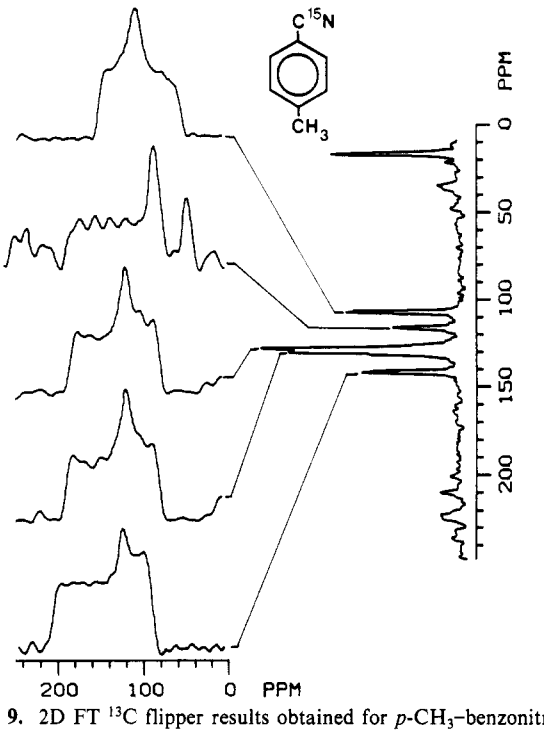

Figure 9. 2D FT ^{13}C flipper results obtained for p-CH_3–benzonitrile.

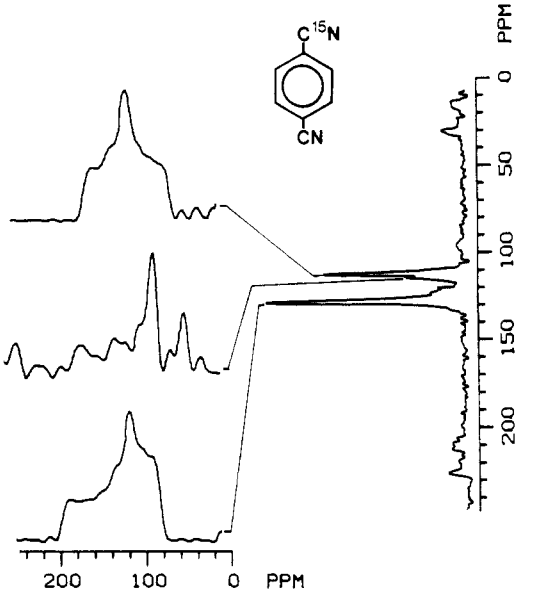

Figure 10. 2D FT ^{13}C flipper results obtained for p-CN–benzonitrile.

2D FT flipper experiments were carried out on para-substituted benzonitriles with the following six substituents: CH_3O–, Me_2N–, O_2N–, NC–, H_3C–, and $I^-Me_3N^+$–. The results are given in Figures 7–12. 2D FT flipper results were not obtained on the Me_3C– derivative, because the melting point of 5–8 °C made it impractical to obtain a true powder pattern by simply cooling the probe. Results were not obtained on the F and Cl derivatives because the ^1H T_1 values were sufficiently long for the compounds, at least 40 s, and also because of poor resolution due to spectral overlap in the F_2 dimension, to render the 2D FT experiments impracticable because of signal-to-noise constraints. For the Br derivative poor resolution and spectral overlap in the F_2 dimension resulted in severe signal-to-noise problems.

The 2D FT flipper spectra shown in Figures 7–12 were all obtained on ^{15}N-labeled samples (99% ^{15}N) in order to avoid effects of dipolar coupling with ^{14}N, which could be substantially

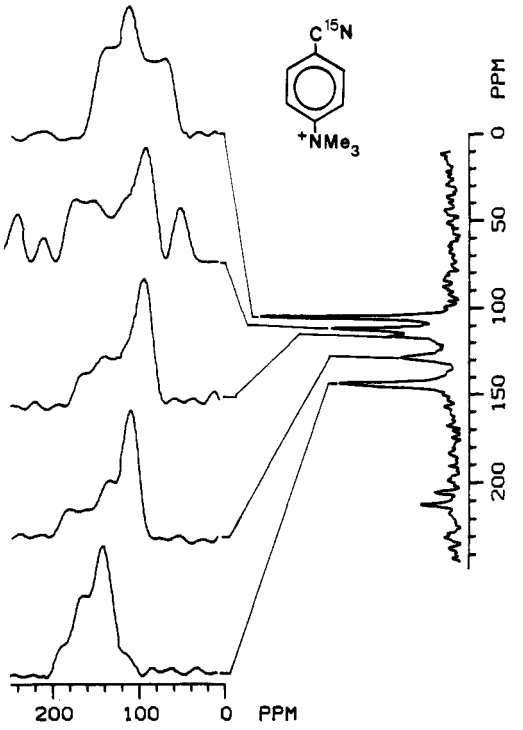

Figure 11. 2D FT ^{13}C flipper results obtained for p-Me_3N^+–benzonitrile.

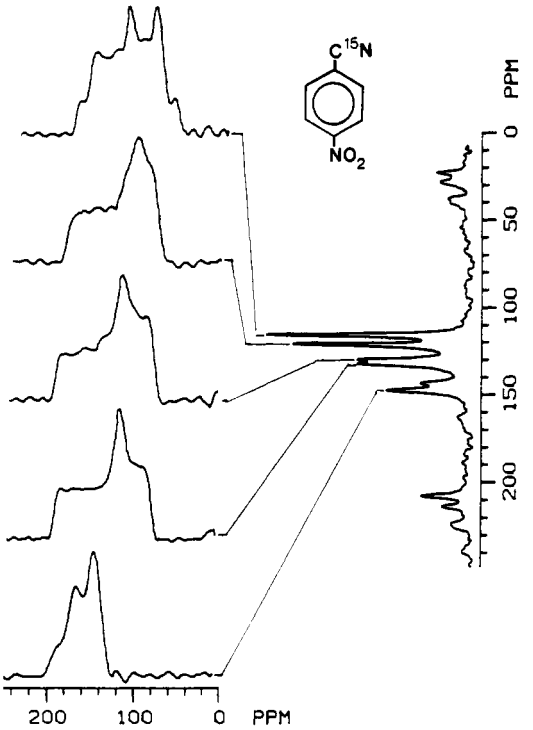

Figure 12. 2D FT ^{13}C flipper results obtained for p-NO_2–benzonitrile.

complicated by the ^{14}N nuclear electric quadrupole interaction, on the observed ^{13}C powder patterns, especially for the C7 carbon resonances. However, for the ^{15}N-labeled case, the dipolar effects of the spin-$^1/_2$ ^{15}N nuclei must be taken into account in interpreting the ^{13}C powder patterns. Figure 13 shows a plot of the ^{13}C–^{15}N dipolar coupling constant

$$D = \hbar\gamma_C\gamma_N/r_{CN}^3 \quad (4)$$

as a function of the ^{13}C–^{15}N internuclear distance r_{CN}. Vertical dashed lines are drawn at r_{CN} values that correspond to the three types of carbons closest to the nitrogen nucleus in a benzonitrile framework. The dipolar coupling constants for these three r_{CN} values are found to be 1980, 250, and 25 Hz, corresponding to 80, 10, and 1 ppm on the ^{13}C shift scale at 25.3 MHz. These three

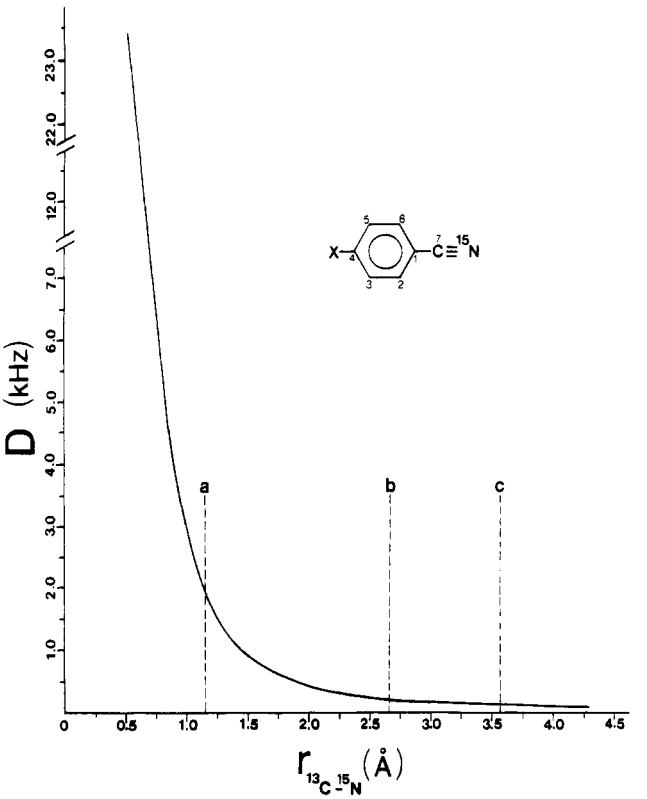

Figure 13. Plot of dipolar coupling (D) vs bond distance $r(^{13}C$–$^{15}N)$, showing vertical lines corresponding to the distances for (a) C7–N, (b) C1–N, and (c) C2,6–N.

values, when the appropriate scaling factor of $-^1/_2$ is taken into account for sample spinning at 90°, are expected to affect the appearance of the C7 powder patterns both qualitatively and quantitatively, the C1 powder patterns quantitatively but not qualitatively, and the C2, C6 powder pattern in no experimentally discernible manner.

In order to take the effects of ^{13}C–^{15}N coupling explicity into account in the powder patterns observed in the F_1 domain of the 2D FT experiments on para-substituted benzonitriles, one has to consider the net ^{13}C powder pattern as the superposition of two component powder patterns, one due to ^{13}C spins experiencing the dipolar interaction with ^{15}N in the $m = ^1/_2$ spin state and the other ^{13}C powder pattern resulting from ^{13}C spins experiencing dipolar interactions with ^{15}N in the $m = -^1/_2$ spin state. The calculation for each component powder pattern is facilitated for the C1 and C7 cases by the fact, dictated by molecular symmetry, that for these carbons the principal axes of both the dipolar and chemical shift tensors can be considered the same. Therefore, for a specific crystallite orientation in a powder pattern, one simply needs to add the computed dipolar contribution (positive or negative) to the chemical shift contribution. The kinds of resulting patterns anticipated for the C7 carbons of para-substituted benzonitriles, after taking the $-^1/_2$ scaling factor of eq 3 into account, are shown in parts c′ and d′ of Figure 1 for the nearly axially symmetric and asymmetric cases, respectively.

One sees from the analysis indicated above, or from inspection of Figure 1, that the net result of the ^{13}C–^{15}N dipolar contribution is to add features that give an overall increased breadth of $3D/4$ to the observed powder pattern ($+D/4$ on the right border and $-D/2$ on the left border). These "corrections" have been made to the results evaluated here for the C7 and C1 powder patterns.

Examination of the ^{13}C powder patterns shown in Figures 7–12 shows indeed that the C7 patterns for some cases (X = NMe_2, OCH_3, CH_3, NO_2) display the more complicated structures expected because of substantial ^{13}C–^{15}N dipolar effects and can be rationalized in terms of the predicted form shown in Figure 1c′ for an axially symmetric or nearly axially symmetric ^{13}C chemical shift tensor. For p-nitrobenzonitrile (Figure 12) the C7 powder pattern is further complicated by the fact that the C1 peak of the

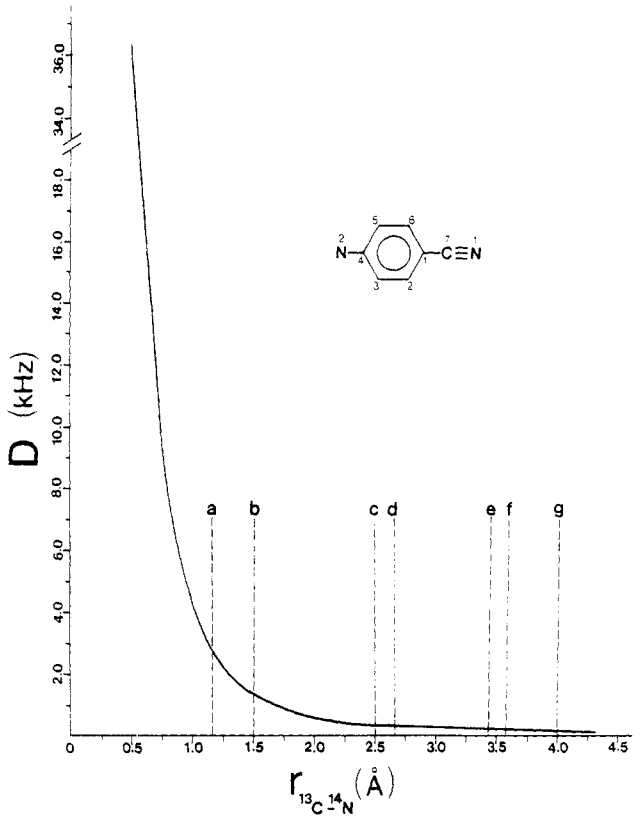

Figure 14. Plot of dipolar coupling (D) vs bond distance, $r(^{13}C-^{14}N)$, showing vertical lines corresponding to distances for (a) C7–N1, (b) C4–N2, (c) C3,5–N2, (d) C1–N1, (e) C2,6–N2, (f) C2,6–N1, and (g) C1–N2.

MAS spectrum in the F_2 domain overlaps with the C7 peak, so the two CSA powder patterns overlap in the F_1 domain. Deconvolution of the features of this powder pattern was made possibly only by means of comparisons with other C1 and C7 powder patterns for this series of compounds.

The derivation of σ_{11}, σ_{22}, and σ_{33} values for most of the other carbon resonance in the para-substituted benzonitriles studied was more straightforward. In the C4 patterns for the cases of Me_3N^+–, Me_2N–, and O_2N– substituents, we see powder patterns that deviate markedly from the anticipated pattern shapes. These are carbon environments in which there is a directly attached ^{14}N atom, from which one should expect some complication in the ^{13}C powder pattern. If one could neglect effects due to deviations of the ^{14}N quantization axis from $\mathbf{B}_0$ because of a strong nuclear electric quadrupolar interaction, and if one could neglect ^{14}N relaxation, then one could estimate the effect of the dipolar interaction of ^{14}N on the ^{13}C powder pattern.

Figure 14, analogous to Figure 13, shows the dependence of ^{14}N–^{13}C dipolar coupling on the ^{13}C–^{14}N internuclear distance (r_{CN}), with vertical lines showing r_{CN} values of particular interest in the present circumstance. We see that for a typical single-bond C–N distance of about 1.5 Å one expects a ^{13}C–^{14}N dipolar splitting of about 1.3 kHz, or 52 ppm on the ^{13}C scale. This could give rise to a major "distortion" of the C4 powder pattern. For C3 and C5 carbons, one can calculate a ^{13}C–^{14}N dipolar coupling of about 300 Hz, or 12 ppm for ^{13}C; this would represent a significant perturbation but one that could be experimentally difficult to identify.

The values of the ^{13}C chemical shift tensor elements obtained by the 2D FT flipper technique are collected in Table III. These values are listed as σ_{aa}, σ_{bb}, and σ_{cc} in order of increasing shielding and can be converted to σ_{11}, σ_{22}, and σ_{33} values by using the definitions stated in eq 2b. For most cases in the present study, application of these definitions shows that $\sigma_{aa} = \sigma_{11}$, $\sigma_{bb} = \sigma_{22}$, and $\sigma_{cc} = \sigma_{33}$. However, for the C1 carbons for the cases, X = Me_2N, CH_3O–, and Me_3N^+–, one finds that $\sigma_{aa} = \sigma_{33}$ and $\sigma_{cc} = \sigma_{11}$, if we choose to follow the definitions in eq 2b explicitly.

As expected, it is seen that none of the ^{13}C chemical shift tensors is axially symmetric ($\eta = 0$), although the values for C7 are rather small (<0.1) for each case. It is also noteworthy that, with the exception of the C4 carbon adjacent to the nitrogen atom in the $-NO_2$ substituent of *p*-nitrobenzonitrile, values of $\sigma_{iso} = {}^1/_3(\sigma_{11} + \sigma_{22} + \sigma_{33})$ calculated directly from the powder patterns are within about 2 ppm of the σ_i values obtained directly in a CP/MAS experiment. This is consistent with our estimation of the reliability of these principal tensor elements at ±3 ppm. The σ_{kk} values listed in Table III for the C4 position of the cases with $-NMe_2$, $-N^+Me_3$ and $-NO_2$ substituents are shown in parentheses to indicate the uncertainties, mentioned above, associated with dipolar interactions with ^{14}N.

The spinning sideband method was also used to obtain σ_{11}, σ_{22}, and σ_{33} values for all the compounds listed in Table I. Sample slow-spinning MAS spectra (obtained with MAS speeds of 1.5–3.5 kHz at 90.5 MHz) are shown in Figure 15. The results of the computational analyses of the SSB patterns are summarized in Table III. For those cases in which both methods were applicable and were not compromised by uncertain contributions from dipolar interactions, one finds qualitative, but not quantitative, agreement between σ_{kk} values obtained by the two methods.

When applying the flipper method, one can account straightforwardly for the effect of ^{15}N dipolar coupling on the ^{13}C powder patterns observed in the F_1 domain, because separate contributing powder patterns associated with the $+{}^1/_2$ and $-{}^1/_2$ ^{15}N spin states are expected in the observed ^{13}C F_1 powder patterns (see Figure 1c′,d′, and Figures 7–12 for C7). By contrast, in the SSB method, the ^{15}N dipolar effects on the modulation patterns in the free induction decay and the corresponding sideband intensities in the Fourier transformed frequency spectra provide no direct way to evaluate *separately* the behaviors of ^{13}C magnetization associated with ^{15}N in the $+{}^1/_2$ and $-{}^1/_2$ spin states (or with ^{14}N in the $m = -1$, 0, and 1 states). Hence, instead of attempting to fit the SSB intensity patterns with respect to the three parameters, σ_{11}, σ_{22}, and σ_{33}, one would have to fit with respect to six such parameters (or nine in the ^{14}N case). As the three-parameter fit is itself difficult in even ideal cases (e.g., one ^{15}N resonance, Table II), attempting a six-parameter fit was deemed unworkable in this project. Accordingly, the C7 σ_{kk} values reported for the SSB method in Table III are enclosed in parentheses in order to call attention to this deficiency in the data. (The reported values were obtained by a SSB analysis carried out as if there were no dipolar interactions involved.) Similar comments are pertinent to the C4 SSB results for X = $-NMe_2$, $-N^+Me_3$, $-NO_2$, and –F.

For both the ^{13}C and ^{15}N chemical shift tensors of the cyano groups in these para-substituted benzonitriles, we assume that molecular symmetry is not likely to be violated seriously by crystal packing "distortions"; in this case symmetry dictates that the principal shielding tensor axes lie as follows: (x) perpendicular to the C–N bond axis and in the plane of the aromatic carbons, (y) perpendicular to the plane of the aromatic carbons, and (z) along the C–N bond axis, as shown diagrammatically in Figure 16. Fung,[25] on the basis of liquid crystal approach, has determined the ^{13}C principal tensor elements of benzonitrile. For the CN carbon he reported the values 231 ± 14, 213 ± 9, and −88 ± 5 ppm and has identified the corresponding principal axis as x, y, and z, respectively. With some variations due to substituent effects, these σ_{kk} values are similar to the values represented in Table III, especially if one excludes for consideration those σ_{kk} values that are enclosed in parentheses, which indicate likely uncertainties associated with effects due to dipolar interactions with ^{15}N or ^{14}N. Indeed, with those exclusions of uncertain results made, it is interesting to note how small the substituent effects are on σ_{aa}, σ_{bb}, or σ_{cc} for the C7 (cyano) carbon. This behavior is in contrast to the 31 (or 41) ppm range of substituent effects found for the ^{15}N σ_{22} values obtained by the static technique (or the SSB method).

It seems likely that the higher sensitivity of the ^{15}N σ_{kk} values than the ^{13}C σ_{kk} values of the –CN group to substituent effects is associated with the expected greater tendency of resonance interactions to alter the local electronic distributions of the nitrogen

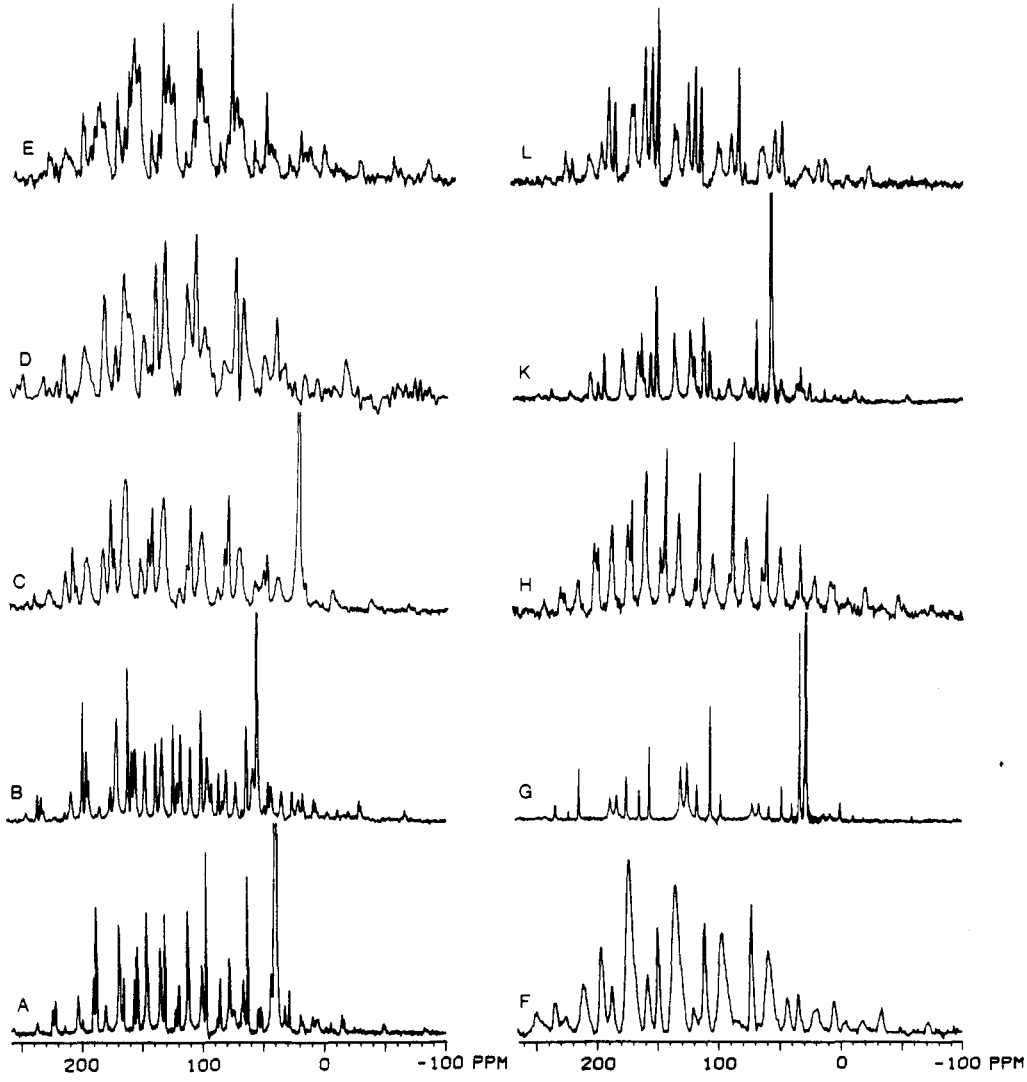

Figure 15. ^{13}C spinning sideband (SSB) spectra of para-substituted benzonitriles: (A) $-NMe_2$, (B) $-OCH_3$, (C) $-CH_3$, (D) -F, (E) -Cl, (F) -Br, (G) $-CMe_3$, (H) -CN, (I) $-N^+Me_3I^-$, (J) $-NO_2$.

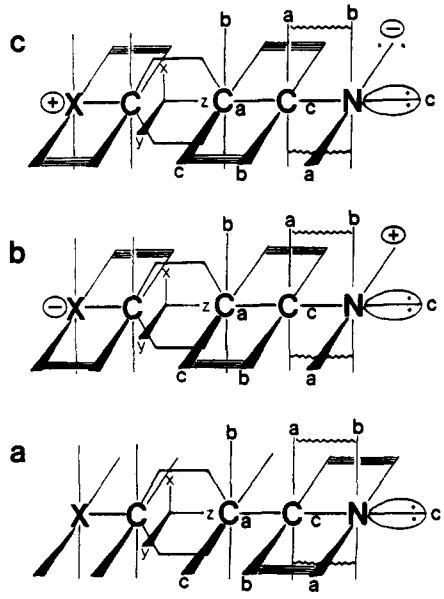

Figure 16. Geometries and axis systems pertinent to this study, showing orbital occupations of the N, C7, C1, C4, and X atoms (orbital occupations of $2p_y$ only shown for C1, C4, and X). The x,y,z axis system is a molecule-fixed system, defined as shown. The a,b,c axes for each atom are defined in terms of the chemical shift elements by $\sigma_{aa} > \sigma_{bb} > \sigma_{cc}$ for each atom. (a) The predominant canonical form. (b) A canonical form describing the effect of a resonance-withdrawing substituent. (c) A canonical form describing the effect of a resonance-donating substituent.

atom, relative to the carbon atom. This is indicated in the resonance structures shown in II.

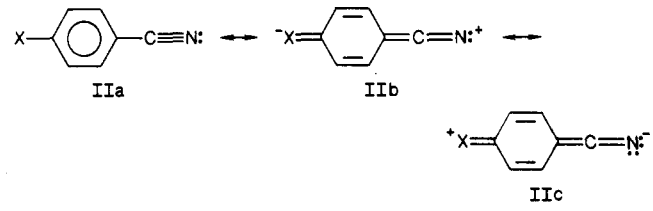

IIa IIb IIc

For the C1 carbons of the para-substituted benzonitriles, local symmetry again dictates that the three principal axes be directed as indicated in Figure 16. For these carbons σ_{aa} varies from 182 to 221 ppm, σ_{bb} varies from 86 to 129 ppm, and σ_{cc} varies from 4 to 30 ppm. These ranges correspond to Fung's[25] values for the corresponding benzonitrile carbon, $\sigma_{aa} = 211$, $\sigma_{bb} = 104$, and $\sigma_{cc} = 23$, which are intermediate values in the ranges observed in the present work. By analogy with other results in the literature on analogous systems, especially Fung's benzonitrile results, we assign σ_{aa} to the principal axis z shown in Figure 16, σ_{bb} to x, and σ_{cc} to y.

For the remaining ring carbons of the para-substituted benzonitriles—C2, C3, C4, C5, and C6—local symmetry dictates that two of the principal axes of the chemical shift tensor lie in the plane of the aromatic carbons, with the remaining one, y, being perpendicular to the plane of the aromatic carbons. For these carbons the σ_{aa} values (corresponding to one of the in-plane axes) obtained in this study vary from 174 to 243 ppm, the σ_{bb} values (corresponding to the other in-plane axis) from 117 to 183 ppm,

and the σ_{cc} values (corresponding to the y axis) from −1 to 68 ppm. Thus, considering all of the aromatic carbons, but taking into account only those numbers not in parentheses, we find σ_{aa}, σ_{bb}, and σ_{cc} ranges of 174–243 ppm (a 69 ppm range), 86–183 ppm (a 97 ppm range) and −1–68 ppm (a 69 ppm range). This same set of carbons yields a range of isotropic ^{13}C chemical shifts of 96–161 ppm, i.e., a 65 ppm range. Thus, each individual σ_{kk} value displays a total range of substituent effects that is slightly larger than does σ_i, and the total range for all three σ_{kk} elements is nearly 4 times as large as the σ_i range.

Empirical Correlations. The most reliable data in Tables II and III (those numbers not enclosed in parentheses) were examined extensively for possible empirical correlations with various electronic and reactivity parameters. NMR data that were examined are the individual σ_{kk} values, as well as σ_{iso}, δ, and η. Electronic/reactivity parameters against which potential empirical correlations were explored are the effective substituent electronegativity[39] and the combination of the reactivity parameters, σ_I and σ_R°.[40] This combination was examined in the form, $C_I\sigma_I + C_R\sigma_R^\circ$,[41] where C_I and C_R are variable parameters to be optimized in a computer least-squares fitting. No high-quality correlations were found. In a few cases "hints" of correlations were encountered, in which a high-quality fit could be obtained if one or two data points were removed. However, in such cases, there was no apparent justification for deleting the "troublesome" points, so these avenues were abandoned.

One can inquire into the reason(s) for the observed absence of simple empirical correlations between the chemical shift tensor data and reactivity parameters. At least two explanations come to mind. First, it is a priori possible that such correlations were not found in the present work simply because the experimental data are not sufficiently accurate or precise to support such correlations. Second, it is possible that, no matter how good the data, there are simply no such correlations to be found! As we have focused on only the most reliable chemical shift data, especially the ^{15}N chemical shift data, in searching for empirical correlations, we do not believe that the first explanation is valid. It seems more likely that empirical correlations of the type examined are simply not "there" to be found.

The absence of general empirical correlations between chemical shift data and reactivity parameters, although they have sometimes been found,[10] should not be surprising. Reactivity parameters depend upon free energy differences between *ground states* of reactants and products (as in the original Hammett ionization constants of substituted benzoic acids[42]) or of reactants and activated complexes (if kinetic data are employed to determine the reactivity parameters). These energies are primarily related to electronic charge distributions in *ground* states and are described in terms of *first-order* electronic properties.[43] Chemical shift tensor elements are *second-order* properties,[43-45] requiring a knowledge of electronic wave functions calculated in the presence of a perturbation (caused by $\mathbf{B}_0$), i.e., requiring in computations a knowledge of *excited*-state wave functions and energies. In the context of a second-order perturbation framework, the chemical shift tensor elements depend on energy differences between the *ground state* and *excited states*, as well as on the electronic wave functions of *both* kinds of states. In view of such fundamental differences, one should not *expect* to find simple correlations between chemical shift parameters and reactivity parameters. In those cases in which such empirical correlations are encountered, they may be of some interest but should not be interpreted as reflecting a fundamental kinship between these very different types of quantities.

Theoretical Considerations. Since the early reformulation by Pople and Karplus[46,47] of Ramsey's work[48] on the theory of ^{13}C chemical shifts, most theoretical discussions of ^{13}C chemical shifts have emphasized the so-called local paramagnetic term $\sigma^{(p)}$ in the overall description of the shielding tensor:

$$\sigma_A = \sigma_A^{(d)} + \sigma_A^{(p)} + \sum_{C \neq A} \sigma_A^{(c)} \quad (5)$$

In this equation, which can be written either for individual tensor elements or for the isotropic average, $\sigma_A^{(d)}$ is a diamagnetic effect resulting from local electronic circulations centered on the Ath carbon atom, $\sigma_A^{(p)}$ is a paramagnetic effect resulting from electronic circulations centered on the Ath carbon atom, and the third sum of terms accounts for the effects that electronic circulations centered on atoms different from atom A have on the shielding of the Ath nucleus. Pople and Karplus[46,47] showed that the local paramagnetic term, $\sigma_A^{(p)}$, is the one that accounts primarily for the chemical shift variations that are observed experimentally for ^{13}C (or, by inference, other nuclides with p and d orbitals in their atomic valence shells); the other terms are usually neglected in qualitative discussions. Our discussions will likewise be based on $\sigma^{(p)}$ contributions to the chemical shift.

Although the most successful computational ^{13}C chemical shift theory has been the ab initio perturbed SCF MO approach,[45] the MO perturbation framework at the independent-electron level, as formulated by Pople,[46] is useful for discussing general structure–shift relationships. This theory provides a direct focus for viewing the electron circulations induced in the molecule by $\mathbf{B}_0$ in terms of electron excitations. For the specific tensor element, $\sigma_{\alpha\alpha}$, of a specific carbon atom, where α,β,γ define Cartesian axes, this theory provides the result for the local paramagnetic terms of eq 5:

$$\sigma_{\alpha\alpha}^{(p)} = -(e^2\hbar^2)/(2m^2c^2)\langle r^{-3}\rangle_{2p} \sum_{j}^{occ} \sum_{k}^{unocc} (\Delta\epsilon_{jk})^{-1}(C_{j\beta A}C_{k\gamma A} - C_{j\gamma A}C_{k\beta A}) \sum_{B \neq A}^{other\ atoms} (C_{j\beta B}C_{k\gamma B} - C_{j\gamma B}C_{k\beta B}) \quad (6)$$

where A is the nucleus for which the shielding tensor is being calculated, e and m are the electronic charge and mass, respectively, and c is the speed of light. In this equation the summation indices j and k cover all the occupied and unoccupied molecular orbitals, respectively, $\Delta\epsilon_{jk}$ is the "excitation energy" between the jth occupied and kth unoccupied MO's, $\langle r^{-3}\rangle_{2p}$ is the expectation value of the inverse cubed distance of an electron from the nucleus in a 2p atomic orbital centered on the carbon atom of interest (A), and $C_{\beta j}$ is the coefficient in the jth MO of the $2p_\beta$ atomic orbital centered on the atom of interest in the summation.

The effects of substituent variations on the ^{13}C chemical shift tensor elements of the individual carbons of a specific molecular framework can be discussed in terms of each of the quantities $C_{\beta j}$, $\langle r^{-3}\rangle_{2p}$, and $\Delta\epsilon_{jk}$. The effects of substituents on the atomic orbital coefficients in the MO's are the effect on which we focus most strongly in the present discussion. The excitation energy, $\Delta\epsilon_{ij}$, can be effected by substituent changes by decreasing or increasing an MO energy if the relevant effective nuclear charges are increased or decreased, respectively.

For the carbon atoms near the substituent of the para-substituted benzonitriles of the present study, especially C4, substituent effects on the ^{13}C chemical shifts can be discussed in terms of a variety of physical–organic and/or quantum mechanical characteristics. The former category includes such diverse concepts as inductive effects, resonance effects, effective electronegativities, field effects, neighbor anisotropy effects, and heavy-atom spin–orbit effects. In moving away from the substituent in the molecular

(39) Inamoto, N.; Masuda, S. *Chem. Lett.* **1982**, 1003.
(40) Chapman, N. B.; Shorter, J. *Advances in Linear Free Energy Relationships*; Plenum: New York, 1972; pp 37–38.
(41) Ehrenson, S.; Brownlee, R. T. C.; Taft, R. W. *Prog. Org. Chem.* **1973**, *10*, 1.
(42) Hammett, L. P. *Physical Organic Chemistry*; McGraw-Hill: New York, 1940; p 186.
(43) Pople, J. A.; McIver, Jr., J. W.; Ostlund, N. S. *J. Chem. Phys.* **1968**, *49*, 2960.
(44) Ellis, P. D.; Maciel, G. E.; McIver, Jr., J. W. *J. Am. Chem. Soc.* **1972**, *94*, 4069.
(45) Ditchfield, R.; Ellis, P. D. In *Topics in Carbon-13 NMR Spectroscopy*; Levy, G. C., Ed.; Wiley: New York, 1974; Vol. 1, p 1.
(46) Pople, J. A. *J. Chem. Phys.* **1962**, *37*, 53, 60.
(47) Karplus, M.; Pople, J. A. *J. Chem. Phys.* **1963**, *38*, 2803.
(48) Ramsey, N. F. *Phys. Rev.* **1950**, *78*, 699.

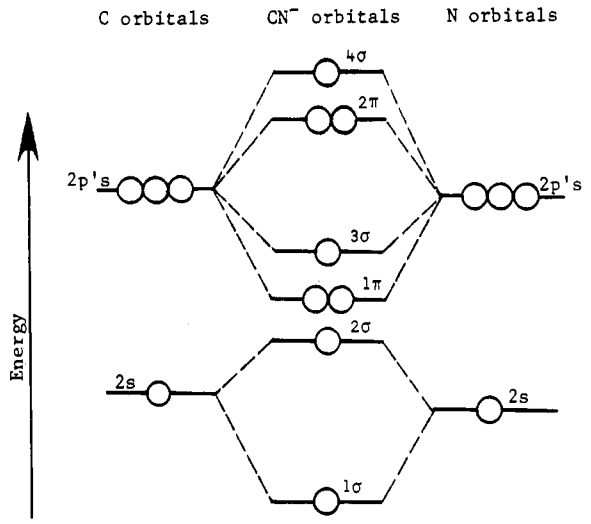

Figure 17. Molecular orbital diagram of CN^-, neglecting the inner-shell electrons and atomic orbitals.

structure, one can expect that most of these concepts will become less important relative to the influence of resonance effects, which by their nature have the potential of exerting long-range influences. Hence, we begin this discussion at the terminal moiety of the structure, the –CN group.

Figure 16 shows the geometrical arrangements of the various atomic orbitals and axis systems pertinent to this discussion. One can see that, in terms of eq 6, it is excitations between the π_x and π_y^* orbitals and between the π_y and π_x^* orbitals that largely determine $\sigma_{zz}^{(p)}$ (σ_{cc} for the nitrogen atom). For $\sigma_{xx}^{(p)}$ (σ_{bb} for N) it is excitations between the occupied sigma (σ) orbitals and π_y^* or between π_y and unoccupied sigma (σ^*) orbitals that are primarily relevant. For $\sigma_{yy}^{(p)}$ (σ_{aa} for N) it is excitations between σ and π_x^* and between π_x and σ^* that are important. Within the limited context of examining shielding tensors for the –CN group, the MO diagram of CN^- (Figure 17) is of interest. From that diagram one sees that $\Delta\epsilon_{ij}$ is much smaller for the $3\sigma \rightarrow 2\pi_x^*$ and $3\sigma \rightarrow 2\pi_y^*$ excitations than for $\pi \rightarrow \pi^*$ excitations, so one expects $\sigma_{xx}^{(p)}$ and $\sigma_{yy}^{(p)}$ to be substantially larger in magnitude than $\sigma_{zz}^{(p)}$ for the nitrogen atom. Therefore, we predict that σ_{aa} and σ_{bb} should be much larger than σ_{cc}, as is found to be the case experimentally (see Table II). Furthermore, as the canonical form of Figure 16a is expected to be dominant, one expects σ_{aa} and σ_{bb} values to be relatively similar.

To the extent that the canonical forms represented in Figure 16b,c are important, reflecting substantial resonance interactions, σ_{aa} and σ_{bb} values might be expected to diverge for the nitrogen atom. For σ_{aa} it is seen that the atomic orbital coefficients of the pertinent MO's are to a first approximation left unchanged by the indicated resonance interactions, IIa ↔ IIb ↔ IIc. For σ_{bb} one sees that these resonance interactions alter directly the nitrogen atom $2p_y$ orbital coefficients of the π_y and π_y^* MO's; hence, we expect substantial substituent effects on σ_{bb}, as found in the experimental results summarized in Table II. A resonance withdrawal, as expected for X = $-NO_2$ and $-C{\equiv}N$, should enhance the relative importance of structure IIb and yield smaller values of the nitrogen atom $2p_y$ orbital coefficient in π_y and correspondingly larger values for π_y^*. Assuming that the larger effect should be that associated with the $\sigma \rightarrow \pi_y^*$ excitation, because of the much smaller $\Delta\epsilon_{ij}$ value (see $3\sigma \rightarrow 2\pi$ in Figure 17), we anticipate an increase in the magnitude of $\sigma_{xx}^{(p)}$ and a corresponding increase in σ_{bb} for resonance withdrawal. This is consistent with the data shown in Table II. A resonance donation, as expected for X = $-NMe_2$ and $-OCH_3$, should enhance the relative importance of structure IIc and yield larger values of the nitrogen atom $2p_y$ orbital coefficient in π_y and correspondingly smaller values for π_y^*. Making the same assumption indicated above for resonance withdrawal, we expect smaller magnitudes for $\sigma_{xx}^{(p)}$ and smaller values for σ_{bb} with resonance donation, as seen in the experimental results of Table II.

For the effect of a resonance-withdrawing substituent on σ_{cc} of the nitrogen atom, the decrease and increase, respectively, of the nitrogen atom $2p_y$ coefficient for the π_y and π_y^* MO's would decrease and increase the effectiveness of the $\pi_y \rightarrow \pi_x^*$ and $\pi_x \rightarrow \pi_y^*$ excitations, respectively. The net result of this should be a relatively small effect on σ_{cc}. A similar prediction is made for the effects of resonance-donating substituents. These predictions are borne out in the relatively small range of substituent effects on σ_{cc} values seen in Table II.

For the C7 (cyano) carbon, an analysis similar to that given above for the nitrogen atom leads again to the conclusion that the tensor element corresponding to the C–N bond axis (σ_{cc}) should be much smaller (higher shielding) than the other two elements, σ_{aa} and σ_{bb}. This pattern is borne out in the experimental data shown in Table III. In this case, the use of a MO diagram of CN^- as a rough framework is more strained, as the cyano carbon experiences strong atomic orbital overlap with the C1 carbon of the ring, which is not represented at all in the MO diagram of CN^-. Examination of Figure 16 shows that the σ_{bb} value of C7 is expected to be largely unaffected by that complication, but σ_{aa} could in some way reflect the direct overlap of the $2p_y$ atomic orbital with that of C1. The fact that η values for C7 in the para-substituted benzonitriles are generally much larger than η values of N of the corresponding compounds is direct evidence of the increased asymmetry associated with this issue.

As explained above, substituent effects on σ_{aa} for C7 should be dominated by effects on $\sigma \rightarrow \pi_y^*$ and $\pi_y \rightarrow \sigma^*$ excitations. If overlap with the C1 $2p_y$ atomic orbital gives rise to significant C7 $2p_y$ participation in π_y and π_y^* orbitals with MO energies for which $\sigma \rightarrow \pi_y^*$ excitation energies are decreased (relative to the corresponding values involving π_x and π_x^*), then $\sigma_{xx}^{(p)}$ would be expected to be larger in magnitude and σ_{xx} would be larger than σ_{yy} for C7. This interpretation is consistent with the results shown in Table III and with MO calculations on simple, relevant R–CN systems.

For C1 and all the other aromatic carbon atoms, the situation is quite different, because of the absence of nearly axial symmetry, as evidenced by the much larger η values shown in Table III. For these carbons, near-planar local symmetry dictates that two of the principal shielding tensor axes lie in the carbon plane of the aromatic ring, and one axis (y) is orthogonal to that plane. For the tensor element corresponding to the y axis (σ_{cc}) the pertinent excitations are those involving $2p_x$ and $2p_z$ atomic orbitals in σ and σ^* MO's. For the elements σ_{aa} and σ_{bb}, the pertinent excitations are those involving $2p_y$ atomic orbitals in π_y or π_y^* MO's and the $2p_x$ and $2p_z$ atomic orbitals in σ and σ^* MO's in the xz plane (σ_{aa}) and along the z axis (σ_{bb}). As the lowest energy $\sigma \rightarrow \sigma^*$ excitations in aromatic systems tend to have larger $\Delta\epsilon$ values than $\sigma \rightarrow \pi^*$ and $\pi \rightarrow \sigma^*$ excitations, it is reasonable that $\sigma_{yy}^{(p)}$ should have a smaller magnitude than $\sigma_{xx}^{(p)}$ or $\sigma_z z^{(p)}$, corresponding to a larger shielding for σ_{cc}; this is what is found in the experimental results shown in Table III. This pattern is also consistent with literature results identifying the principal tensor axes of aromatic rings from single-crystal measurements[17,38] or from theoretical calculations.[44] Although these literature reports also identify σ_{aa} (the lowest shielding element) with the z axis and σ_{bb} (intermediate shielding element) with the x axis for the specific compounds of those studies, it is possible that, for one or more of the para-substituted benzonitriles represented in Table III, there could be a permutation of the $a = z$ and $b = x$ indentifications.

As indicated above, substituent variations can also be expected to influence the $\sigma_{\alpha\alpha}^{(p)}$ values represented in eq 6 via the quantities $\langle r^{-3}\rangle_{2p}$ and $\Delta\epsilon_{jk}$. The quantity, $\langle r^{-3}\rangle_{2p}$, can be influenced by substituent variations via substituent effects on the local electron density[44] and hence effective nuclear charge, of the carbon atom of interest, as described by Slater's screening rules.[49] This factor influences the size of a 2p orbital; e.g., a decreased or increased electron density contracts or expands, respectively, the atomic orbital and increases or decreases $\langle r^{-3}\rangle_{2p}$ accordingly. Pople and Karplus[46,47] and others[44] have noted the importance of this factor

(49) Slater, J. C. *Phys. Rev.* **1930**, *36*, 57.

in determining $\sigma_{\alpha\alpha}^{(p)}$ values, and one should expect that a more complete treatment of substituent effects on σ_{kk} values than the present work would take this issue into account. Similar arguments regarding substituent effects on the effective nuclear charge, and its effect on energy eigenvalues, could be made in terms of the $\Delta\epsilon_{jk}$ values of eq 6. Of course, in a SCF-MO calculation with a suitably extended basis set, this issue is accounted for automatically in the calculation of the eigenvalues and eigenvectors. In any case, this issue is considered to be beyond the scope or level of sophistication of the interpretations of the present paper.

As stated above, the interpretation of ^{13}C σ_{kk} data in terms of simple chemical and physical concepts is increasingly difficult for carbon atoms closer to the substituent, as additional factors, such as inductive effects, field effects, and neighbor anisotropy effects, must be considered. For this reason specific discussion of the C2, C3, C4, C5, and C6 data is not included here.

Conclusions

The principal elements of the chemical shift tensors obtained for ^{15}N and ^{13}C in a variety of para-substituted benzonitriles show a wide range of substituent-dependent values and present a variety of experimental difficulties. For one-line spectra (e.g., ^{15}N in the present case) the static powder pattern provides the most reliable approach for determining σ_{kk} values. For more complex, multiline cases, either the 2D FT flipper technique or the spinning sideband (SSB) MAS approach can be used, each with its advantages and disadvantages. For a large number of closely spaced isotropic-average peaks, it can be difficult or impossible to obtain clearly defined and nonoverlapping SSB patterns. The 2D FT flipper approach circumvents this problem but suffers from signal-to-noise difficulties. By extrapolation it appears that, for highly complex spectra, the 2D flipper approach may be the only currently available technique that is applicable. All of these methods can suffer from the effects of dipole–dipole interactions with nearby nuclei; this problem is especially serious for nearby quadrupolar nuclei, for which dipolar corrections are extremely difficult, at best. There is a clear need for new and improved techniques to supplement or replace the SSB and 2D FT flipper approaches, so that accurate σ_{kk} determinations can be made on sufficiently varied types of samples in sufficiently varied contexts to permit a good assessment of the extent to which the determination of σ_{11}, σ_{22}, and σ_{33} indeed provides a much more useful level of information than the measurement of simply σ_{iso} values.

The measured substituent effects on ^{15}N and ^{13}C σ_{kk} values of para-substituted benzonitriles do not correlate with traditional reactivity parameters, probably reflecting the much different characteristics and dependences on fundamental structural properties of chemical shift and reactivity parameters. The gross structural dependences and patterns of substituent trends of σ_{kk} values can be explained qualitatively, especially for ^{15}N, in terms of Pople's MO perturbation theory of shielding.

Acknowledgment. We gratefully acknowledge support of this research by National Science Foundation Grant CHE-8610151 and use of the Colorado State University Regional NMR Center, funded by National Science Foundation Grant CHE-8616437. We also are very grateful to Prof. Paul Ellis of the University of South Carolina for providing a copy of his computer program for analyzing spinning sideband data and to Prof. A. K. Rappe and J. Iwamiya for assistance with the molecular orbital calculations.

Registry No. *p*-$MeOC_6H_4CHO$, 123-11-5; *p*-$Me_2NC_6H_4CHO$, 100-10-7; *p*-$O_2NC_6H_4CHO$, 555-16-8; *p*-NCC_6H_4CHO, 105-07-7; *p*-ClC_6H_4CHO, 104-88-1; *p*-BrC_6H_4CHO, 1122-91-4; *p*-FC_6H_4COCl, 403-43-0; *p*-MeC_6H_4COCl, 874-60-2; *p*-$(Me)_3CC_6H_4COCl$, 1710-98-1; *p*-$FC_6H_4CONH_2$, 824-75-9; *p*-$MeC_6H_4CONH_2$, 619-55-6; *p*-$(Me)_3CC_6H_4CONH_2$, 56108-12-4; *p*-methoxybenzonitrile, 874-90-8; *p*-dimethylaminobenzonitrile, 1197-19-9; *p*-nitrobenzonitrile, 619-72-7; *p*-dicyanobenzene, 623-26-7; *p*-chlorobenzonitrile, 623-03-0; *p*-bromobenzonitrile, 623-00-7; *p*-fluorobenzonitrile, 1194-02-1; *p*-methylbenzonitrile, 104-85-8; *p-tert*-butylbenzonitrile, 4210-32-6; *p*-cyanophenyltrimethylammonium iodide, 17311-01-2.

Infrared Laser-Induced Reaction of Ethyl Isocyanide: Comparison with Methyl Isocyanide

L. M. Yam, M. J. Shultz,* Elizabeth J. Rock,† and Susanne Buchau†

Department of Chemistry, Tufts University, Medford, Massachusetts 02155 *(Received: December 29, 1986; In Final Form: March 4, 1988)*

Results from the infrared laser-induced reaction of ethyl isocyanide indicate the overall behavior to be similar to that of methyl isocyanide with some significant differences. Similarities include the following: (1) both exhibit a dramatic dependence of nitrile yield on reactant pressure, including a threshold pressure above which massive isomerization occurs; (2) this threshold pressure is not due to a thermal explosion; (3) both contain a radical channel along with the isomerization channel. Major differences between the methyl isocyanide and ethyl isocyanide reactions are attributable to the nature of the radicals in the particular isocyanide system.

In the past decade, interest in infrared laser-induced chemical reactions centered on the quest for mode selectivity. This interest was sparked by work on laser isotope separation in the 1970s.[1,2] In much of this work it is common to find a strongly increasing yield with fluence. However, it is much less common to find an increase with pressure, particularly in a substrate that does not show evidence of saturation. The most dramatic example of an increasing yield with pressure is the IR laser-induced reaction of methyl isocyanide.[3-5]

This work extends the previous methyl isocyanide investigation to ethyl isocyanide, which contains nine additional vibrational degrees of freedom. These extra vibrations will illustrate the effect of increasing the density of states on the reaction. Note that the activation energy (38.24 kcal/mol)[6] and enthalpy of reaction

†Department of Chemistry, Wellesley College, Wellesley, MA 02181.

(1) Ambartzumian, R. V.; Letokhov, V. S.; Rayabov, E. A.; Chekalin, N. V. *JETP Lett. (Engl. Transl.)* **1974**, *20*, 273.
(2) Lyman, J. L.; Jensen, R. J.; Rink, J.; Robinson, C. P.; Rockwood, S. D. *Appl. Phys. Lett.* **1975**, *27*, 87.
(3) Shultz, M. J.; Rock, E. J.; Tricca, R. E.; Yam, L. M. *J. Phys. Chem.* **1984**, *88*, 5157.
(4) Shultz, M. J.; Tricca, R. E.; Yam, L. M. *J. Phys. Chem.* **1985**, *89*, 58.
(5) Shultz, M. J.; Tricca, R. E.; Berets, S. L.; Kostas, C.; Yam, L. M. *J. Phys. Chem.* **1985**, *89*, 3113.
(6) Maloney, K. M.; Rabinovitch, B. S. *J. Phys. Chem.* **1969**, *73*, 1652.

0022-3654/88/2092-4632$01.50/0 © 1988 American Chemical Society